Title
Unified Lateral Motion Control Of Vehicles For Lane Change Maneuvers In Automated Highway Systems

Authors
Chee, Wonshik
Tomizuka, Masayoshi

Publication Date
1997

CALIFORNIA PATH PROGRAM
INSTITUTE OF TRANSPORTATION STUDIES
UNIVERSITY OF CALIFORNIA, BERKELEY

Unified Lateral Motion Control of Vehicles for Lane Change Maneuvers in Automated Highway Systems

Wonshik Chee
Masayoshi Tomizuka
University of California, Berkeley

California PATH Research Report
UCB-ITS-PRR-97-29

This work was performed as part of the California PATH Program of the University of California, in cooperation with the State of California Business, Transportation, and Housing Agency, Department of Transportation; and the United States Department of Transportation, Federal Highway Administration.

July 1997

ISSN 1055-1425

Unified Lateral Motion Control of Vehicles for Lane Change Maneuvers in Automated Highway Systems

Unified Lateral Motion Control of Vehicles for Lane Change Maneuvers in Automated Highways

Wonshik Chee, Graduate Student Researcher
Masayoshi Tomizuka, Professor

Department of Mechanical Engineering
University of California, Berkeley, CA **94720**

PATH Research Report, MOU **89**

Abstract

This report deals with the lateral guidance of vehicles in Intelligent Vehicle Highway Systems (IVHS) with the main emphasis on the lane change maneuvers. In this study, the lateral position of the vehicle is assumed to be measured using the magnetic road reference system, which consists of magnetometers installed on the vehicle and magnets embedded in highway. In addition, a yaw rate sensor and an accelerometer are assumed to be installed on vehicles.

Two approaches are studied for the lane change maneuvers in IVHS; one is to treat the maneuvers as a tracking control problem, and the other is to use the unified lateral guidance algorithm proposed in this report. In the tracking control approach, the desired trajectory for the lane change maneuvers, called the virtual desired trajectory (VDT), is designed considering the lateral acceleration and the lateral jerk for passengers' ride comfort. A sliding mode controller is used as the tracking controller. To enhance passengers' ride comfort, the sliding surface is constructed with respect to the filtered tracking error, which results in smoother control action than the standard sliding mode controller. A reduced order Kalman filter is designed to provide the estimates of the state variables of a vehicle, which are required to implement the sliding mode controller. This approach is validated by experiments performed on a full size vehicle.

The unified lateral guidance algorithm consists of the desired yaw rate generator and the yaw rate tracking controller. The desired yaw rate generator provides the yaw rate tracking controller with the desired yaw rate to achieve the desired maneuvers, either lane change maneuvers or lane following maneuvers. Therefore, the same control algorithm may be applied to the two types of maneuvers. The desired yaw rate for lane following maneuvers is obtained by analyzing the kinematics of the lateral position measurement from the magnetic road reference system. The desired yaw rate for lane change maneuvers is obtained from the virtual desired trajectory. A mode switching algorithm for smooth transitions from the lane change maneuvers to the lane following maneuvers, and vice versa, is proposed. Simulation results validate this approach.

Keywords: Automated Highway Systems, Lateral Motion Control, Lane Change Maneuvers, Unified Lateral Guidance,

Executive Summary

In this report, the lane change maneuvers are studied in two ways: one is to treat the maneuvers as a tracking control problem, and the other is to use the unified lateral guidance algorithm. In the tracking control approach, the desired trajectory for the lane change maneuvers, called the virtual desired trajectory (VDT), is designed considering the lateral acceleration and the lateral jerk for passengers' ride comfort. The trapezoidal acceleration trajectory is proposed as the VDT, and the design of appropriate trapezoidal acceleration can be achieved by compromising the lateral jerk, lateral acceleration and the maneuvering time. The sliding mode control is proposed as the tracking controller to make the vehicle to follow the VDT. In order for the sliding mode controller not to cause adverse effect on the passengers' ride comfort, the sliding surface is constructed with respect to the filtered tracking error, which results in the frequency dependent weight on the tracking error. **A** reduced order Kalman filter is designed to provide the estimates of the state variables of a vehicle which are required to implement the sliding mode controller. This approach is validated by experiments performed on a full size car at Richmond Field Station, University of California at Berkeley.

In order to achieve smooth transitions between the lane change maneuvers and the lane following maneuvers, the unified lateral guidance algorithm is proposed. The unified lateral guidance algorithm consists of the desired yaw rate generator and the yaw rate tracking controller. The desired yaw rate generator provides the yaw rate tracking controller with the desired yaw rate to achieve the desired maneuvers, either lane changing or lane following maneuvers. Therefore, the same control algorithm may be applied to the two types of maneuvers. The desired yaw rate for lane following maneuvers is obtained by analyzing the kinematics of the lateral position measurement from the magnetic road reference system. The desired yaw rate for lane change maneuvers is obtained from the virtual desired trajectory. **A** mode switching algorithm for smooth transitions from the lane change maneuvers to the lane following maneuvers, and vice versa, is proposed. Stability of the overall system was proven. Simulations support the validity of the proposed algorithm.

Chapter 1

Introduction

1.1 Objectives

The California Partners for Advanced Transit and Highways Program (PATH) was launched in 1986, and has been leading the research in Intelligent Transportation Systems (ITS) or its predecessor Intelligent Vehicle Highway Systems (IVHS). The goal of PATH is to develop the foundations for the advanced technologies that will help increase highway capacity, resolve congestion of highways, enhance driving safety, save energy and reduce pollution.

Under the above stated goals, PATH activities are subdivided into three broad categories:

- ATMIS - Advanced Transportation Management Information Systems;
- AVCS - Advanced Vehicle Control Systems;
- Systems - the cross-cutting and institutional issues that apply to both ATMIS and AVCS.

Among the activities, the AVCS includes the lateral motion control of a vehicle to be investigated in this report.

To realize the lateral motion control, the reference sensing and the vehicle state sensing systems are essential. Under the PATH program, the road reference sensing system based on magnets and magnetometers has been extensively studied[40]. It consists of the magnets embedded in highways and the magnetometers installed on vehicles to

measure the magnetic field generated by the embedded magnets. The vehicle lateral position is then obtained from a table indexed by the measured magnetic fields. Additionally, a yaw rate sensor and accelerometers are used as on-board sensors.

The lateral motion control problem consists of lane following maneuvers and lane change maneuvers. The main focuses of this report are the lane change maneuvers using the magnetic reference sensing system. The objective of the lane change maneuvers is to design a control system that controls a vehicle to move from one lane to the adjacent lane using only on-board sensors without jerky switching to and from the lane following controller. One of the significant differences in the lane change maneuvers from the lane following maneuvers is the fact that the road reference system is not available during the lane change maneuvers. Thus, the lane change maneuvers are performed in an open loop manner in the sense that the lateral position measurement is not available.

In this report, the lane change maneuvers in AHS are investigated in two ways; one is to treat the maneuvers as a tracking control problem, and the other is to use the unified lateral guidance algorithm. For the tracking control approach, the desired trajectory for the lane change maneuvers, called the virtual desired trajectory (VDT), is designed by considering passengers' ride comfort. Then, a tracking controller is designed to follow VDT.

The unified lateral guidance algorithm consists of two modules that are connected in a cascaded structure: the yaw rate generation module and the yaw rate tracking control module. The yaw rate generation module generates the desired yaw rate to achieve a desired maneuver, i.e., lane change maneuver or lane following maneuver. Then, the desired yaw rate is realized by the yaw rate tracking controller. The unified lateral guidance algorithm is advantageous because it allows one to design a lateral motion controller for various maneuvers and various sensors through the unified design step without redesigning the feedback controller. This advantage becomes evident in the PATH scenario. In longitudinal control, a set of vehicles is controlled to keep their

spacing automatically. The set of vehicles behaves like a string; this set is called a platoon. In the platoon, the spacing between vehicles is too small to use the visual measurement because most of the image is blocked by the preceding vehicle. Therefore, a hybrid use of the visual measurement and the magnetic sensors is desirable. To realize the hybrid sensing system, the lateral control system should be designed for each sensing system and combined to accommodate various situations. This control system design can be simplified by the proposed unified lateral guidance algorithm. By designing the desired yaw rate from the kinematics of each measurement, the control system design is completed. Thus, the lateral control of a vehicle under various scenarios can be achieved in the unified way by designing the yaw rate generation module in series with the yaw rate tracking controller.

1.2 Previous Work

In this section, a literature review of the research related to the topics covered in this report is presented.

Vehicle Modeling

Lateral motion dynamics of a vehicle have been studied since the late 1950's. A three-degree-of-freedom vehicle model, which includes the yaw, lateral, and roll motions, was developed by Segel[31]. It suggested that the longitudinal velocity of a vehicle should be considered as a major parameter for its stability. A simpler model, usually called the bicycle model, was then developed by neglecting the roll motion([9][32][37]). For the purpose of controller design, the bicycle model has been acknowledged to be sufficiently accurate and widely used ([3][9][15][22][25][27]). More complex models with a larger number of degree-of-freedoms have been also developed for realistic simulation studies([20][26]).

Lane Following Maneuvers

In the late 1950's, GM and RCA conducted research on the lane following maneuvers [11]. Fenton et. al. used classic frequency domain control theory to design a controller for the lane following maneuvers. Their design was verified by experiments[9]. Ackermann utilized robust control theory based on the parameter space to design an automatic steering system for vehicles with the lateral position measurement using the continuous wire embedded in highways[2].

In the PATH program, linear lateral motion controllers, using frequency shaped linear quadratic (FSLQ) optimal control theory and the optimal preview control theory, have been developed ([25][26][27][28]). In addition, a fuzzy rule-based controller has been designed. The effectiveness of these controllers has been verified by experiments ([15][16][27]).

To deal with various uncertainties in road-tire interaction, sliding mode control approaches to steering control have been proposed in Pham et. al.[29] and Ackermann et. al. [3]. Pham et. al. used a saturation function in place of a sign function in the standard sliding mode control in order to avoid the chattering problem[34]. Ackermann et. al. proposed a two stage design: in the first stage, the desired yaw rate is obtained so that the measured lateral position converges to zero, and in the second stage a sliding control law is constructed to force the yaw rate to follow the desired value obtained from the first stage. This two stage design was originally proposed by Pappas et. al.[23] for the lateral guidance of vehicle-like robots. In his work, the unicycle model was used to represent the dynamics of the vehicle-like robot at low velocities where the no slip condition was assured.

Lane Change Maneuvers

In contrast to lane following maneuvers, considerably less research has been conducted for lane change maneuvers. Godthelp et al.[12] investigated human driving patterns and reported that steering angle variations during lane change maneuvers resemble sine functions and that lane change maneuvers may be divided into four stages according to the signs of steering angle and its time derivative. A preview control model of a human driver during lane following maneuvers and lane change maneuvers was proposed by Hess and Modjtahezadeh([13][14][21]). Chee and Tomizuka proposed the FSLQ controller and the sliding mode controller for lane change maneuvers, and showed the effectiveness of the control algorithms by simulations([5][6]). Experimental results were presented in [7] to show the effectiveness of the controller and the estimation scheme.

1.3 Organization of the Report

This report is organized as follows. In Chapter 2, some preliminaries for the vehicle lateral guidance are discussed. The simplified vehicle model, the new algorithm for road reference sensing system and VDT are discussed in Chapter2. In Chapter 3, the lane change maneuvers are treated as a tracking control of VDT. The tracking controller is designed via sliding mode control theory, and a reduced order Kalman filter is proposed as a state estimator. Some analyses of the tracking error and experimental results are presented. In Chapter 4, the unified lateral guidance algorithm is proposed, and applied to the lateral guidance under the PATH scenario. The stability of the overall system is proven, and the effectiveness of the proposed algorithm is confirmed by simulations. Finally, conclusions are drawn in Chapter 5.

Chapter 2

Preliminaries for Lateral Guidance of a Vehicle

In this chapter, the lateral guidance (or lateral motion control) of a vehicle, including lane change maneuvers and lane following maneuvers, is explained in the context of intelligent vehicle highway systems (IVHS). Then, the vehicle model is discussed from the control point of view. The new algorithm to get the lateral position from the magnetic road reference sensing system is presented in detail. Finally, the desired trajectory for the lane change maneuvers is proposed.

2.1 Lateral Guidance System for IVHS

Increasing highway congestion, resulting in gridlock, deteriorating effects on the environment through inefficient use of fuel, and hazardous driving conditions, has inspired a great deal of research interest in the intelligent vehicle highway systems (IVHS). The underlying goals of the IVHS include the reduction of highway congestion, improvement of driving safety, and reduction of pollution.

The lateral guidance of a vehicle falls into the category of advanced vehicle control systems (AVCS). The goal of the AVCS in the IVHS context is to achieve complete driving automation. Thus, the lateral guidance system should be able to execute both the lane change maneuvers and lane following maneuvers. The concept of the two maneuvers is depicted in Figure 2.1.

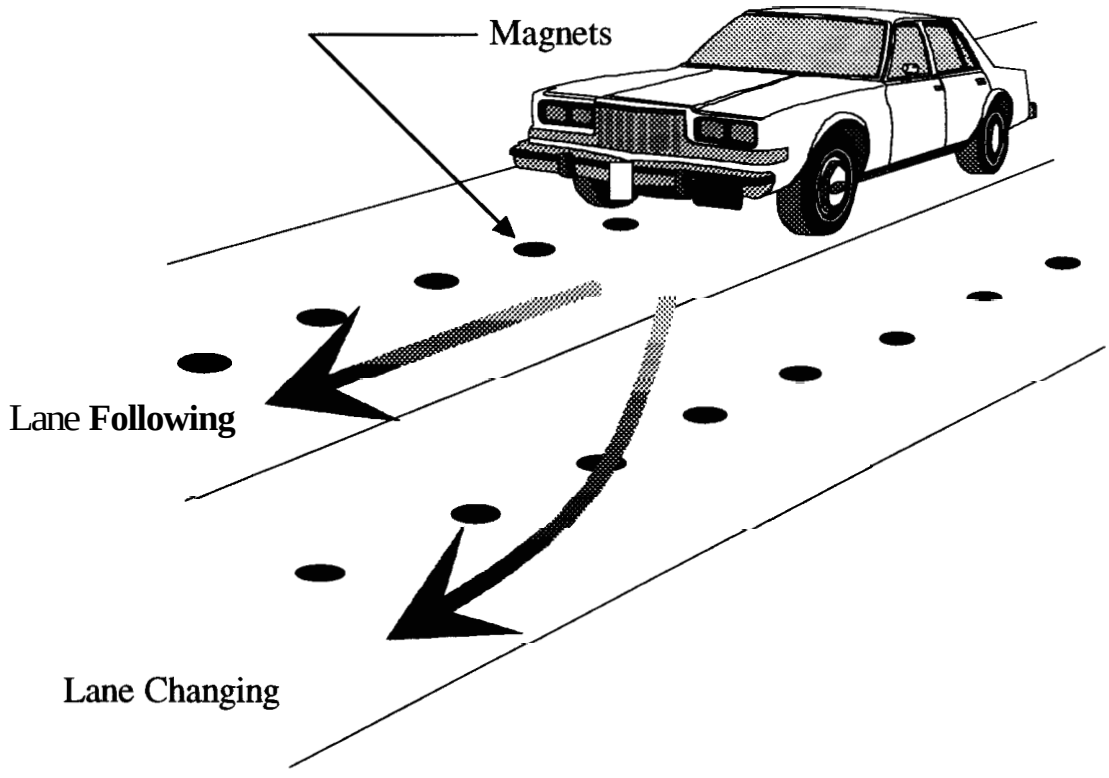

Figure 2.1: Concept of Maneuvers

The task of the lane following maneuvers is to control a vehicle to follow the road reference sensing system. As shown in Figure 2.1, the road reference sensing system in PATH is based on magnets embedded in highway lanes. The lane following maneuvers can be treated as a tracking problem since the lateral position of the vehicle, which represents a tracking error, is always available. Many works on the vehicle lateral guidance have been devoted to the lane following maneuvers as mentioned in Chapter 1.

The objective of the lane change maneuver in IVHS is to control a vehicle to move from the current lane to the adjacent lane(Figure 2.1). One important issue in the magnet based lateral guidance is the availability of the lateral position measurement. Since the vehicle passes the region where the magnetic fields generated by the embedded magnets are not detectable during the lane change maneuvers, the maneuver may have to be conducted in an open loop manner without lateral position measurement. In such cases,

the lateral position of a vehicle should be estimated using the information from on-board sensors, such as yaw rate sensors and accelerometers.

Another important issue is the transition from a lane change maneuver to a lane following maneuver and vice versa. Since the lateral position is available only during lane following maneuvers, the control algorithm for lane change maneuvers needs to accommodate such data switching. A smooth transition algorithm will be discussed later.

2.2 Bicycle Model

In this section, we discuss the dynamics of the vehicle for controller design. The bicycle model is used to design control and estimation algorithms presented in the later chapters. The bicycle model represents vehicle motions in a horizontal plane. It is obtained by lumping the two front and the two rear wheels into one front and one rear wheels in the center line of the vehicle, and by neglecting suspension dynamics. Thus, the roll, pitch, and heave motions are not included.

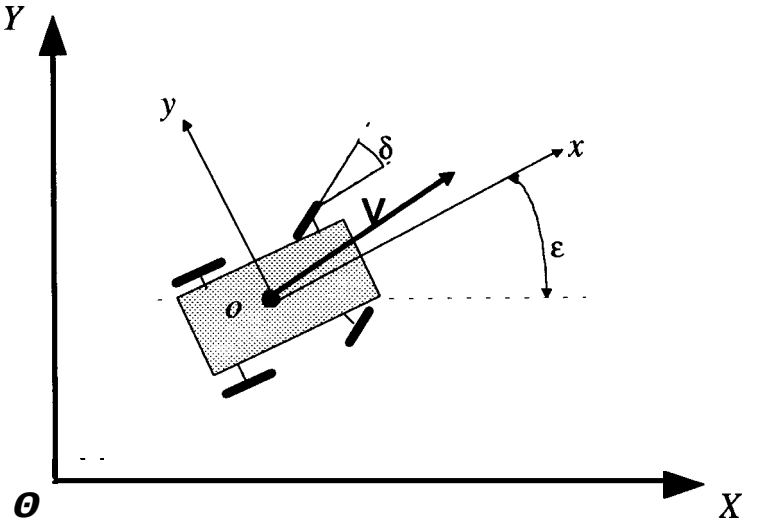

Figure 2.2: Coordinates for Bicycle Model

Referring to Figure 2.2, and assuming a constant longitudinal speed (V_x), the equations of motion using the axes fixed to the vehicle **(oxy)** can be written as follows.

$$m(\dot{V}_y + V_x\dot{\varepsilon}) = f_f \cos 6 + f_r \tag{2.1}$$

$$I_z\ddot{\varepsilon} = 1, f_f \cos 6 - l_2 f_r \tag{2.2}$$

In these equations, V_x denotes the speed in the direction of **ox** axis and V_y the one in the direction of **oy** axis. The velocity of a vehicle, **V,** is obtained from V_x and V_y. ε denotes the yaw angle with respect to the absolute coordinates, *OXY,* and δ represents the steering angle of the vehicle. Other symbols and their nominal values are listed in Table 2.1. f_f and f_r are the side forces for the front tire and the rear tire, respectively.

Table 2.1: Variables and Parameters of Model

δ	front steering wheel angle
ε	yaw angle of the vehicle (or Ψ)
V	longitudinal speed of the vehicle (31.1 *m*/sec)
C_s	cornering stiffness (40000 *N/rad*)
m	mass of the vehicle (1720 *kg*)
I_z	moment of inertia of the vehicle (3250 kgm^2)
l_1	distance from c.g. to front axle (1.137 *m*)
l_2	distance from c.g. to rear axle (1.530 *m*)

It is noted that the side force in each tire is a function of tire side slip angle. The slip angle is defined as the angle between the direction of an object and the velocity vector of the object. If the object is a tire, we can obtain the tire slip angle as follows.

$$a, = 6 - \frac{l,\& + V_y}{V_x} \tag{2.3}$$

$$a, = \frac{l_2\dot{\varepsilon} - V_y}{V_x} \tag{2.4}$$

Here, α_f and α_r represent the front and the rear tire side slip angle, respectively. Now, the side force can be represented as follows.

$$f_f = f_f(\alpha_f) \tag{2.5}$$

$$f_r = f_r(\alpha_r) \tag{2.6}$$

If we assume the tire slip angles are small, the side forces are written as

$$f_f = 2C_s\alpha_f \tag{2.7}$$

$$f_r = 2C_s\alpha_r . \tag{2.8}$$

Then, the linearized bicycle model can be written as

$$m(\dot{V}_y + V_x\dot{\varepsilon}) = 2C_s\delta - \frac{2C_s(l_1 - l_2)}{V_x}\dot{\varepsilon} - \frac{4C_s}{V_x}V_y \tag{2.9}$$

$$I_z\ddot{\varepsilon} = 2l_1C_s\delta - \frac{2C_s(l_1^2 + l_2^2)}{V_x}\dot{\varepsilon} - \frac{2C_s(l_1 - l_2)}{V_x}V_y . \tag{2.10}$$

This linearized model will be used in the later chapters.

2.3 Desired Trajectory for Lane Change Maneuvers

In the study of lane change maneuvers, we assume that the maneuvers are performed on the automated lanes, on which magnets are installed at every lm. The objective of the lane change maneuver is to make the vehicle move laterally from one lane to the adjacent lane using on-board computer and sensors. One of the key performance objectives of the maneuvers is to maintain ride comfort throughout the maneuvering period under any reasonable environmental uncertainties, such as road surface conditions and lateral wind conditions.

In order to achieve the performance objective, the desired trajectory for the lane change maneuvers is designed to minimize the lateral acceleration and lateral jerk that are generated when the vehicle exactly follows the trajectory under the specified values. Several trajectories have been studied previously[5]. Among the trajectories proposed in

[5], the trapezoidal acceleration trajectory is chosen as the desired trajectory in this dissertation.

For the trapezoidal acceleration trajectory, the acceleration profile is specified as shown in Figure 2.3. Here, the jerk corresponds to the slope of the acceleration profile.

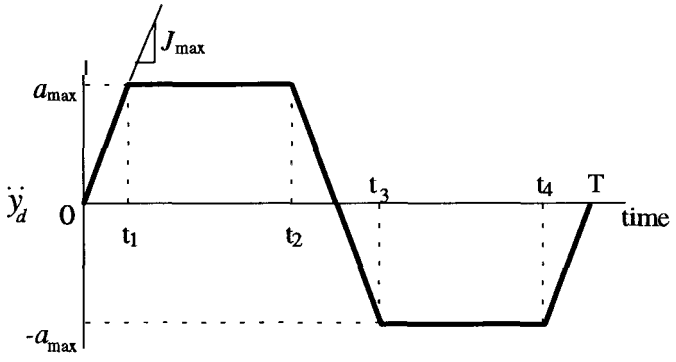

Figure 2.3: Trapezoidal Acceleration Profile

From this figure, the desired lateral acceleration, $\ddot{y}_d$, can be written as

$$\begin{aligned}\ddot{y}_d &= J_{max} t \cdot u(t) - J_{max}(t-t_1)\cdot u(t-t_1) - J_{max}(t-t_2)\cdot u(t-t_2) \\ &+ J_{max}(t-t_3)\cdot u(t-t_3) + J_{max}(t-t_4)\cdot u(t-t_4) - J_{max}(t-T)\cdot u(t-T)\end{aligned} \tag{2.11}$$

where, J_{max} is the jerk limit and $u(t)$ is the unit step function. Temporal parameters for this trajectory, t_1, t_2, t_3, t_4, and T can be obtained by integrating equation (2.11) twice with respect to time and setting $y_d(T) = d$ with zero initial conditions. Then, the lateral position can be written as

$$y_d = \frac{J_{max}}{6}\left\{\begin{matrix} t^3 \cdot u(t) - (t-t_1)^3 \cdot u(t-t_1) - (t-t_2)^3 \cdot u(t-t_2) \\ + (t-t_3)^3 \cdot u(t-t_3) + (t-t_4)^3 \cdot u(t-t_4) - (t-T)^3 \cdot u(t-T) \end{matrix}\right\} \tag{2.12}$$

The parameters of the trajectory are obtained as follow.

$$\begin{aligned} t_1 &= \frac{a_{max}}{J_{max}}, \quad t_2 = \frac{-t_1^2 + \sqrt{t_1^4 + 4t_1 \dfrac{d}{J_{max}}}}{2t_1} \\ t_3 &= 2t_1 + t_2, \quad t_4 = t_1 + 2t_2, \quad T = 2t_1 + 2t_2 \end{aligned} \tag{2.13}$$

Note that the parameters, t_1, t_2, t_3, and t_4 as well as T, depend on $\frac{a_{max}}{J_{max}}$. Several trajectories with different values of the acceleration limit for the same lateral jerk limit, 0.1g/sec, are shown in Figure 2.4. Here, the longest time trajectory is for 0.1g, and the shortest time trajectory is for 0.4g. Between the two extreme trajectories, other trajectories are designed with increments by 0.1g.

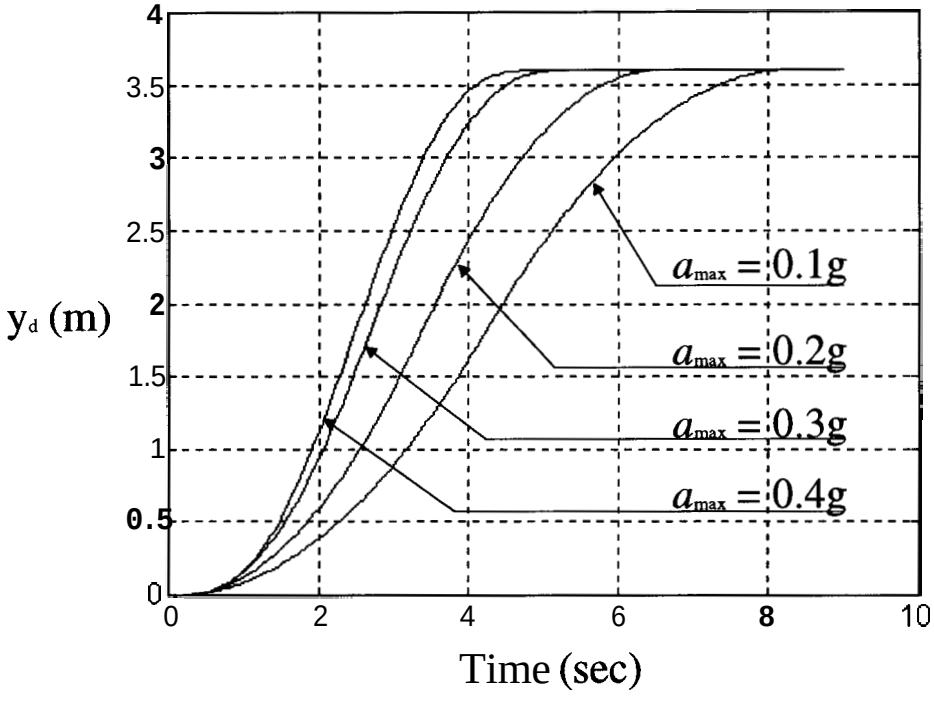

Figure 2.4: Trapezoidal Acceleration Trajectories ($J_{max} = 0.1g/sec$)

To obtain the maneuvering time as a function of the lateral jerk and acceleration limits, t_2 should be expressed as

$$t_2 = -\frac{1}{2}\frac{a_{max}}{J_{max}} + \frac{1}{2}\sqrt{\left(\frac{a_{max}}{J_{max}}\right)^2 + 4\frac{d}{a_{max}}}. \tag{2.14}$$

Then, the maneuvering time, T, can be written as

$$T = 2(t_1 + t_2) = \frac{a_{max}}{J_{max}} + \sqrt{\left(\frac{a_{max}}{J_{max}}\right)^2 + 4\frac{d}{a_{max}}} \tag{2.15}$$

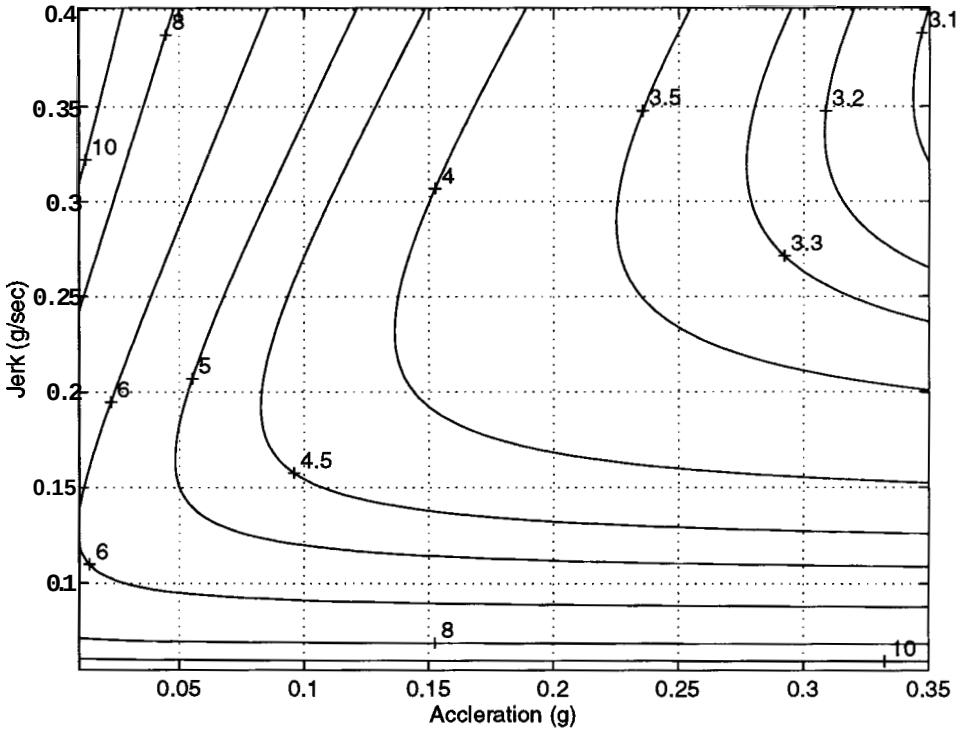

Figure 2.5: Transition Time vs. Lateral Acceleration and Lateral Jerk

The transition time for various accelerations and jerks is shown in Figure 2.5. In this contour plot, the numbers on contours represent the transition time as shown in equation (2.15). Figure 2.5 can be used as a design tool for the virtual desired trajectories. For example, if one wants to design a trajectory with 4-second transition time and $0.15g$ lateral acceleration, then the jerk limit is read as $0.3g/sec$ from Figure 2.5. With the lateral acceleration and the jerk value, one can obtain the desired trajectory from (2.12). The trapezoidal acceleration trajectory is easy to parameterize, and it allows us to find the optimal trade-off between the maneuvering time and the specification of the ride comfort constraints. Thus, it may be the most practical and desirable candidate for the VDT of lane change maneuvers. In the rest of this dissertation, the trapezoidal acceleration trajectory will be selected as the VDT.

2.4 Summary

This chapter covered the preliminary information regarding the vehicle model, concept of maneuvers, lateral position sensing algorithm and the desired trajectory of the lane change maneuvers. The new lateral position sensing algorithm was validated by experimental results. Compared with the algorithm proposed in [40], the new algorithm provides wider measurement range and an increased number of the sensed positions, and is simpler to implement. The desired trajectory for the lane change maneuvers was designed with the consideration of ride comfort. Since the positions are not measurable, this trajectory is called "virtual" desired trajectory (VDT).

Chapter 3

Lane Change Maneuvers - Tracking Control Formulation

In this chapter, lane change maneuvers for the automated highway systems are treated as a tracking control problem with the virtual desired trajectory (VDT) proposed in Chapter **2.** The tracking controller to follow the desired trajectory is designed based on the sliding mode control theory. **A** filter is cascaded with the tracking error to include the frequency dependent weightings in order to enhance passenger ride comfort[6]. These frequency dependent weightings can be interpreted as frequency shaping of the sliding mode found in [39]. Since the controller is a state feedback controller, a reduced order Kalman filter[38] is designed to estimate the lateral position and the lateral velocity that are not measurable. Experimental results validate this strategy for lane change maneuvers.

3.1 Vehicle Model for Controller Design

For the control algorithm design and the estimation algorithm design, the bicycle model[37] mentioned in Section **2.2** is used. *As* a tracking problem, the controller is designed for the vehicle to follow the VDT introduced in Chapter **2.** The tracking error is defined as the difference between **y,** shown in Figure 3.1 and the desired lateral position obtained from the VDT. Here, the vehicle model is expressed in terms of y, and the yaw angle ε to simplify the controller design.

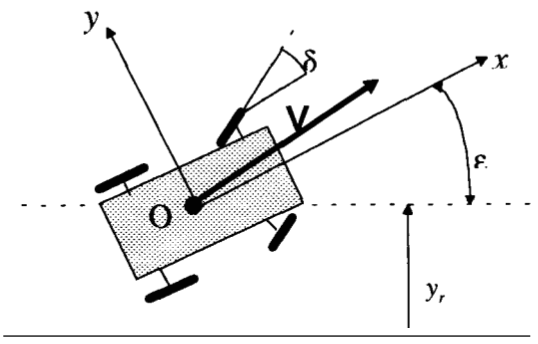

Figure 3.1: Definition of Variables

The equations of lateral and yaw motions of a vehicle mentioned in Chapter 2 are written as

$$m\left(\dot{V}_y + V_x\dot{\varepsilon}\right) = 2C_s\delta - \frac{2C_s\left(l_1 - l_2\right)}{V_x}\dot{\varepsilon} - \frac{4C_s}{V_x}V_y \tag{3.1}$$

$$I_z\ddot{\varepsilon} = 2l_1C_s\delta - \frac{2C_s\left(l_1^2 + l_2^2\right)}{V_x}\& \frac{2C_s\left(l_1 - l_2\right)}{V_x}V_y. \tag{3.2}$$

In these equations, V_x denotes the speed in the direction of the ox axis, and V_y is the speed in the direction of the oy axis. V_x and V_y constitute the velocity of a vehicle, **V.** Yaw angle is denoted by ε, and δ represents the steering angle of a vehicle. Other symbols and their nominal values are listed in Table 2.1.

From Figure 3.1, $\dot{y}_r$ can be related to V_x, V_y, and yaw by

$$\dot{y}_r = V_y \cos\varepsilon + V_x \sin\varepsilon \tag{3.3}$$

Assuming that $\varepsilon = o(1)$, **(3.3)** can be approximated as follows.

$$\dot{y}_r \approx V_y + V_x\varepsilon \tag{3.4}$$

Additionally assuming that V_x is constant (= V), $\ddot{y}_r$ becomes

$$\ddot{y}_r \approx V_y + V_x\dot{\varepsilon} \tag{3.5}$$

By using (3.4)and (3.5), and denoting V_x by V, equations (3.1)and (3.2) can be written as

$$\ddot{y}_r = \frac{A_1}{V}\dot{y}_r - A_1\varepsilon + \frac{A_2}{V}\dot{\varepsilon} + B_1\delta - \frac{K_y}{m}\{V_{wy} + \dot{y}_r - V\varepsilon\}\left|V_{wy} + \dot{y}_r - V\varepsilon\right| \tag{3.6}$$

$$\ddot{\varepsilon} = \frac{A_3}{V}\dot{y}_r - A_3\varepsilon + \frac{A_4}{V}\dot{\varepsilon} + B_2\delta \tag{3.7}$$

The last term in the right hand side of equation (3.6) represents the lateral wind drag. Here, A_i's and B_i are defined as follows.

$$\begin{aligned} A_1 &= \frac{-4.0C_s}{m}, A_2 = \frac{-2.0C_s(E, -l_2)}{m}, A_3 = \frac{-2.0C_s(l_1 - l_2)}{I_z} \\ A_4 &= \frac{-2.0C_s(l_1^2 - l_2^2)}{I_z}, B_1 = \frac{2.0C_s}{m}, \text{and} \quad B_2 = \frac{2.0C_s l_1}{I_z} \end{aligned} \tag{3.8}$$

The uncertainty bounds on A_i's and B_i's can be derived by expanding them as follows[5].

$$\begin{aligned} A_1 &= \hat{A}_1(1+\Delta A_1), A_2 = \hat{A}_2(1+\Delta A_2), A_3 = \hat{A}_3(1+\Delta A_3) \\ A_4 &= \hat{A}_4(1+\Delta A_4), B_1 = \hat{B}_1(1+\Delta B_1), B_2 = \hat{B}_2(1+\Delta B_2) \end{aligned} \tag{3.9}$$

Here, $\hat{A}_i$ and $\hat{B}_i$ denote their nominal values, while ΔA_i and ΔB_i represent the multiplicative uncertainty terms.

Table 3.1: Possible Ranges of Parameters

Cornering Stiffness (C_s)	$0.2 \sim 1.0 C_{s\,\text{nominal}}$
Mass (m)	$0.85 \sim 1.15 m_{\text{nominal}}$
Moment of Inertia about Vertical Axis (I_z)	$0.85 \sim 1.15 I_{z\,\text{nominal}}$

Considering the ranges of the parameters shown in Table 3.1, we find that these uncertainty terms are bounded by

$$\begin{aligned} &|\Delta A_i| \le \alpha \quad , \quad 1 \le i \le 4 \\ &|\Delta B_j| \le \beta \quad , \quad 1 \le j \le 2 \\ &\alpha = \beta = 0.8261 \end{aligned} \tag{3.10}$$

Details of the derivation can be found in Section 3.5. These bounds are used in the design of the sliding mode controller.

3.2 Design of Control Algorithm

Since the simplified model described by equation **(3.6)** includes a nonlinear term, the sliding mode controller is designed as the tracking controller for the VDT. The sliding mode controller is an effective nonlinear controller in the presence of uncertainties and disturbances. Due to its high gain controller characteristics, the sliding mode controller shows several undesirable consequences. One of them is a large control input when the tracking error is large. To reduce large and rapid variation of the control input, a filter is implemented in the following development.

The tracking error is defined as

$$e(t) = \{y_r(t) - y_d(t)\} + \varpi\{\varepsilon(t) - \varepsilon_d(t)\} \tag{3.11}$$

where, y_d and ε_d are the desired lateral position and the desired yaw angle of the vehicle obtained from the VDT. Here, ϖ is a dimension conversion factor and weighting factor as well. In the following, ϖ is assumed to be 1 for the convenience of the calculations.

The sliding surface is defined as

$$S(t) = \left(\frac{d}{dt} + \lambda\right)^2 v(t) = 0 \tag{3.12}$$

where, $v(t)$ is the filtered tracking error satisfying

$$\frac{dv(t)}{dt} \ln\gamma \cdot v(t) = e(t), \quad 0 < \gamma < 1.0 \,. \tag{3.13}$$

Note that $v(t)$ can be viewed as the weighted integral of the tracking error:

$$v(t) = \int_0^t \gamma^{(t-\tau)} e(\tau) d\tau \,. \tag{3.14}$$

Convergence of the tracking error to zero when $S(t) = 0$ is proved in Section **3.6.**

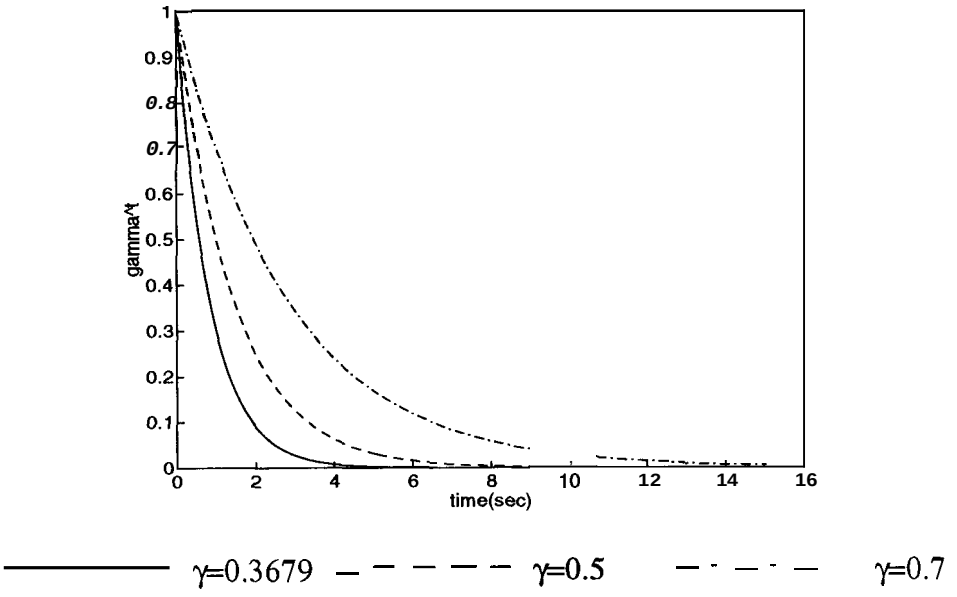

Figure 3.2: Impulse Response of Filter

Figure 3.2 shows the impulse response of the filter for some selected values of γ. When $\gamma = 1.0$, the impulse response becomes a unit step function, and $v(t)$ represents the integral of the tracking error, which has been suggested in the design of sliding mode controllers by several researches ([29][34]). Therefore, an integration can be interpreted as a convolution with the filter whose impulse response is a constant, i.e., a filter that equally emphasizes all the past errors. With $0 < \gamma < 1.0$, the impulse response places more weights on near-past errors than far-past errors. Thus, $v(t)$ implies the weighted integration of the tracking error with emphasis on the near-past errors. These relatively light weights on far-past errors imply a forgetting action.

The stability of the sliding surface ($S(t) = 0$) can be guaranteed by the sliding condition([34][36]).

$$\frac{1}{2}\frac{d}{dt}\left(S^2\right) < -\eta \cdot |S| \tag{3.15}$$

However, this ideal sliding condition requires the discontinuity of the control law across the sliding surface. To remove the discontinuity, a boundary layer with thickness Φ can be introduced([34][39]). This implies that, for $|S| \geq \Phi$, equation (3.15) is attempted, and, for $|S| < \Phi$,

$$\frac{1}{2}\frac{d}{dt}\left(S^2\right) < -\frac{\eta}{\Phi}S^2 . \tag{3.16}$$

This condition has the advantage in that it does not require the discontinuity mentioned above. Its drawback is that $S(t) = 0$ is not achieved in the presence of disturbance. A remedy for this problem is to include the integral of the tracking error, i.e., $\gamma = 1$ in the equation (3.14).

The control input that satisfies the ideal sliding condition (3.15) is

$$\delta = \frac{1}{\hat{B}_1 + \hat{B}_2}\left\{-\frac{\left(\hat{A}_1 + \hat{A}_3\right)}{V}y_r + \left(\hat{A}_1 + \hat{A}_3\right)\varepsilon - \frac{\left(\hat{A}_2 + \hat{A}_4\right)}{V}\dot{\varepsilon} + \frac{K_y}{\hat{m}}\left(\dot{y}_r - V\varepsilon\right)\left|\dot{y}_r - V\varepsilon\right|\right. \tag{3.17}$$
$$\left. + \ddot{y}_d + \ddot{\varepsilon}_d - \left(2\lambda + \ln\gamma\right)\dot{e} - \left(\lambda + \ln\gamma\right)^2 e - \ln\gamma\cdot\left(\lambda + \ln\gamma\right)^2 v - K\cdot\mathrm{sgn}(S)\right\}$$

In this equation, K denotes the robust term which cancels the system uncertainties, and is given by

$$K = \eta + 2\alpha\left|\frac{\left(\hat{A}_1 + \hat{A}_3\right)}{V}y_r - \left(\hat{A}_1 + \hat{A}_3\right)\varepsilon + \frac{\left(\hat{A}_2 + \hat{A}_4\right)}{V}\dot{\varepsilon}\right|$$
$$+ \frac{K_y}{\hat{m}}\left\{V^2 w_m + \left[2V w_m + \alpha\left|\dot{y}_r - V\varepsilon\right|\right]\left|\dot{y}_r - V\varepsilon\right|\right\} \tag{3.18}$$
$$+ \alpha\left|\ddot{y}_d + \ddot{\varepsilon}_d - \left(2\lambda + \ln\gamma\right)\dot{e} - \left(\lambda + \ln\gamma\right)^2 e - \ln\gamma\left(\lambda + \ln\gamma\right)^2 v\right|$$

where, a is the system uncertainty bound obtained from equation (3.10). Derivation of equations (3.17) and (3.18) can be found in Section 3.7.

The control input which will satisfy the condition (3.16) is still given by equations (3.17) and (3.18). However, $\mathrm{sgn}(S)$ in equation (3.17) is now replaced by the saturation function defined as

$$sat\left(\frac{S}{\Phi}\right)=\begin{cases}\dfrac{S}{\Phi}, & \text{for } |S|<\Phi \\ \operatorname{sgn}\left(\dfrac{S}{\Phi}\right), & \text{for } |S|\geq\Phi\end{cases} \tag{3.19}$$

Due to the steady state error caused by this saturation function, the value of y is bounded below by the allowable steady state error. From the ride comfort consideration, we can find the upper bound for γ. Combining these two bounds, we can obtain

$$e^{-\frac{\xi}{K_{\max}}\zeta} \leqq \gamma \leq e^{-\sqrt{1-\Omega_l^2}} \tag{3.20}$$

The detailed derivation of (3.20) is in Section 3.8.

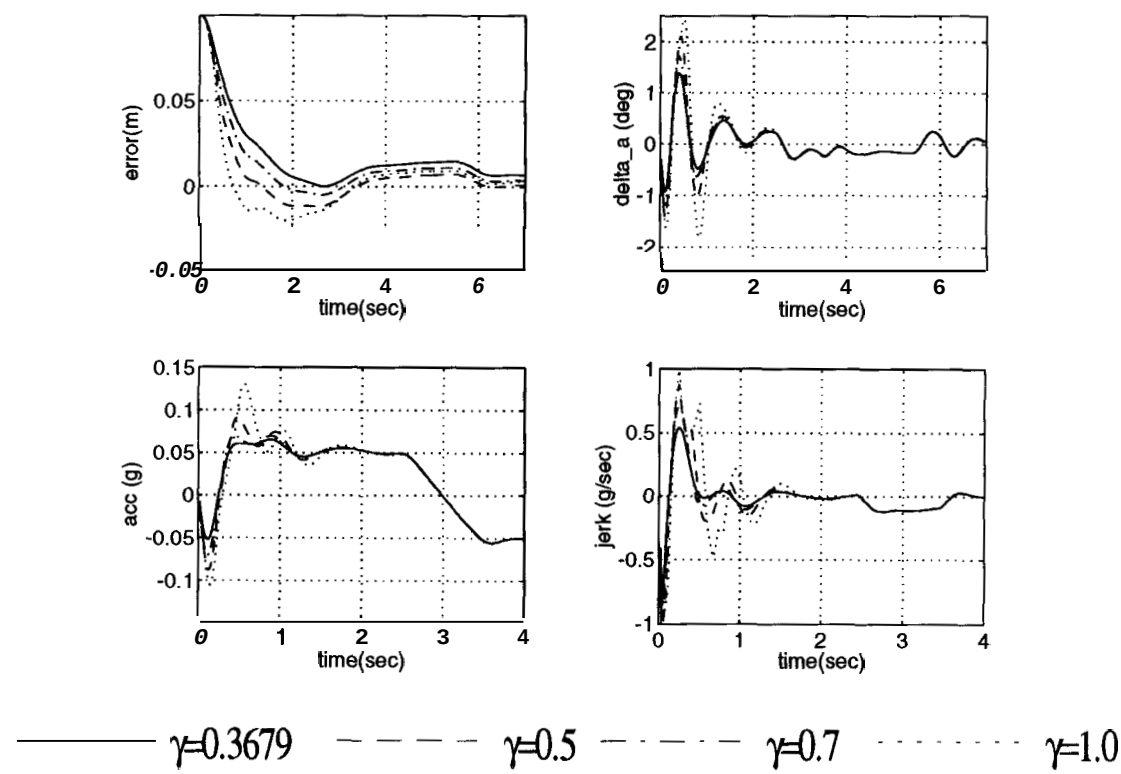

Figure 3.3: Effect of Filter Constant y (Simulation)

Figure **3.3** shows the effect of the filter constant y on the system performance when the cornering stiffness is set to 50% of its nominal value, which represents slippery road condition. The initial lateral error is $0.1m$. In this figure, the upper left plot shows

the tracking error relative to the VDT, and the upper right plot shows the steering wheel angle. The lower two plots show the lateral acceleration and the lateral jerk, respectively. As can be seen in the figure, the peak values of the steering wheel angle (δ) are reduced as γ becomes smaller, especially over the time interval, 0 - 1 sec. Consequently, the acceleration and the jerk are also reduced, which means ride comfort enhancement. However, the tracking error near the end of the maneuver tends to be bigger as γ is reduced.

Therefore, the filter makes the control input smooth, and the vehicle responds with smaller peaks of the lateral acceleration and jerk at the expense of tracking performance.

3.3 Design of State Estimator

Since the lateral position of a vehicle is not directly measurable during lane change maneuvers, a state estimator using on-board sensors (a lateral accelerometer and a yaw rate sensor) is necessary. A Kalman filter is designed based on the linearized model of a vehicle. Its purpose is to estimate the necessary states for control, such as lateral position, lateral speed and yaw angle.

From equations (3.6) and (3.7), the linearized model can be written in the state space form as

$$\dot{\mathbf{x}} = \mathbf{A}\mathbf{x} + \mathbf{B}\delta + \mathbf{B}w \tag{3.21}$$

where,

$$\mathbf{x} = \begin{bmatrix} x_1 & x_2 & x_3 & x_4 \end{bmatrix}^{\mathrm{T}} = [y, \quad \mathbf{y} \quad E \quad \dot{\varepsilon}]^{T} \tag{3.22}$$

$$\mathbf{A} = \begin{bmatrix} 0 & 1 & 0 & 0 \\ 0 & \frac{A_1}{V} & -A_1 & \frac{A_2}{V} \\ 0 & 0 & 0 & 1 \\ 0 & \frac{A_3}{V} & -A_3 & \frac{A_4}{V} \end{bmatrix}, \quad \mathbf{B} = \begin{bmatrix} 0 \\ B_1 \\ 0 \\ B_2 \end{bmatrix}. \tag{3.23}$$

Here, w denotes the system disturbance whose variance is σ_w^2. Since σ_w^2 is not available, it is used as one of the design parameters of the estimator. Measurements from a lateral accelerometer and a yaw rate sensor are written as

$$\mathbf{y} = \mathbf{C} \cdot \mathbf{x} + \mathbf{D}\delta + v \tag{3.24}$$

where,

$$\mathbf{y} = [\text{lateral acceleration (scalar)} \quad \text{yaw rate (scalar)}]^T$$

$$\mathbf{C} = \begin{bmatrix} 0 & \frac{A_1}{V} & -A_1 & \frac{A_2}{V} - V \\ 0 & 0 & 0 & 1 \end{bmatrix}, \quad \mathbf{D} = \begin{bmatrix} B_1 \\ 0 \end{bmatrix}. \tag{3.25}$$

Here, v is the sensor noise vector which is assumed to be white with the following covariance matrix

$$\mathbf{V} = diag\left\{\sigma_{\text{acc}}^2, \quad \sigma_{\text{yaw}}^2\right\} \tag{3.26}$$

where, σ_{acc}^2 and σ_{yaw}^2 denote the variance of lateral accelerometer noise and that of the yaw rate sensor noise, respectively. Note that the measured lateral acceleration is the same quantity denoted by V_y in equations (3.1) and (3.2).

Since the linearized system is unobservable, we decompose the system into the observable part and the unobservable part [17]. Then, by designing the Kalman filter for the observable subsystem, we can obtain a reduced order Kalman filter [38]. The unobservable subsystem is estimated by an open loop estimator.

The estimate of the original state can be represented as

$$\hat{\mathbf{x}} = \mathbf{M}\begin{bmatrix} \hat{\mathbf{x}}_o \\ \hat{\mathbf{x}}_{uo} \end{bmatrix} \tag{3.27}$$

where $\hat{x}_o$ and $\hat{x}_{uo}$ are the observable and the unobservable state components respectively, and $\mathbf{M}^{-1}$ is a nonsingular matrix that transforms the original system into the decomposed system. The details of a procedure to obtain this matrix can be found in [17] and [38].

The estimator for the decomposed system is written as

$$\dot{\hat{\mathbf{x}}}_T = \mathbf{A}_T\hat{\mathbf{x}}_T + \mathbf{B}_T\delta + \mathbf{P}\mathbf{C}_T^T\mathbf{V}^{-1}\{\mathbf{Y} - \mathbf{C}_T\hat{\mathbf{x}}_T - \mathbf{D}\mathbf{S}\} \tag{3.28}$$

where,

$$\hat{\mathbf{x}}_T = \begin{bmatrix} \hat{\mathbf{x}}_o \\ \hat{\mathbf{x}}_{uo} \end{bmatrix} \tag{3.29}$$

$$\mathbf{A}_T = \mathbf{N}\mathbf{A}\mathbf{M} = \begin{bmatrix} \mathbf{A}_1 & 0 \\ \mathbf{A}_{21} & \mathbf{A}_2 \end{bmatrix}, \quad \mathbf{B}_T = \mathbf{N}\mathbf{B} = \begin{bmatrix} \mathbf{B}_1 \\ \mathbf{B}_2 \end{bmatrix}$$
$$\mathbf{C}_T = \mathbf{C}\mathbf{M} = [\mathbf{C}_1 \quad \mathbf{C}_2], \quad \mathbf{N} = \mathbf{M}^{-1} \tag{3.30}$$

The matrix $\mathbf{P}$ satisfies the following algebraic Ricatti equation.

$$0 = \mathbf{A}_T\mathbf{P} + \mathbf{P}\mathbf{A}_T^T - \mathbf{P}\mathbf{C}_T^T\mathbf{V}^{-1}\mathbf{C}_T\mathbf{P} + \mathbf{B}_T\mathbf{W}\mathbf{B}_T^T \tag{3.31}$$

Note that the order of this Ricatti equation is 4×4.

By partitioning $\mathbf{P}$ as

$$\mathbf{P} = \begin{bmatrix} \mathbf{P}_1 & \mathbf{P}_{21} \\ \mathbf{P}_{21} & \mathbf{P}_2 \end{bmatrix},$$

(Note that order of each submatrix is 2×2), we can obtain the state estimates as follows.

$$\begin{aligned} \dot{\hat{\mathbf{x}}}_o &= \mathbf{A}_1\hat{\mathbf{x}}_o + \mathbf{B}_1\delta + \mathbf{P}_1\mathbf{C}_1^T\mathbf{V}^{-1}\{\mathbf{y} - \mathbf{C}_1\hat{\mathbf{x}}_o - \mathbf{D}\mathbf{S}\} \\ \dot{\hat{\mathbf{x}}}_{uo} &= \mathbf{A}_2\hat{\mathbf{x}}_{uo} + \mathbf{A}_{21}\hat{\mathbf{x}}_o + \mathbf{B}_o\delta + \mathbf{P}_{21}\mathbf{C}_1^T\mathbf{V}^{-1}\{\mathbf{y} - \mathbf{C}_1\hat{\mathbf{x}}_o - \mathbf{D}\delta\} \end{aligned} \tag{3.32}$$

where, $\mathbf{P}_1$ and $\mathbf{P}_{21}$ satisfy

$$\begin{aligned} 0 &= \mathbf{A}_1\mathbf{P}_1 + \mathbf{P}_1\mathbf{A}_1^T - \mathbf{P}_1\mathbf{C}_1^T\mathbf{V}^{-1}\mathbf{C}_1\mathbf{P}_1 + \mathbf{B}_1\mathbf{W}\mathbf{B}_1^T \\ 0 &= \mathbf{A}_1\mathbf{P}_{21} + \mathbf{P}_{21}\mathbf{A}_2^T - \mathbf{P}_1\mathbf{C}_1^T\mathbf{V}^{-1}\mathbf{C}_1\mathbf{P}_{21} + \mathbf{B}_1\mathbf{W}\mathbf{B}_2^T \end{aligned} \tag{3.33}$$

Instead of solving the full order equation (3.31), we can obtain the estimates of the original states by solving partitioned system (3.32) and (3.33). Note that the order of each equation in (3.33) is 2×2, which implies the reduction in number of computation.

3.4 Experimental Results

To validate the control algorithm and the state estimation algorithm in the previous chapters, experimental tests were conducted on a PONTIAC 6000 STE sedan at Richmond Field Station **(RFS)** of the University of California at Berkeley. Figure **3.4** depicts the arrangement of the experimental equipment. Here, the on-board sensors include a yaw rate sensor and an accelerometer, and are installed at the center of gravity of the vehicle. The sampling time of the system was 10 msec and the command signal to the front wheel steering actuator was updated at the same sampling rate.

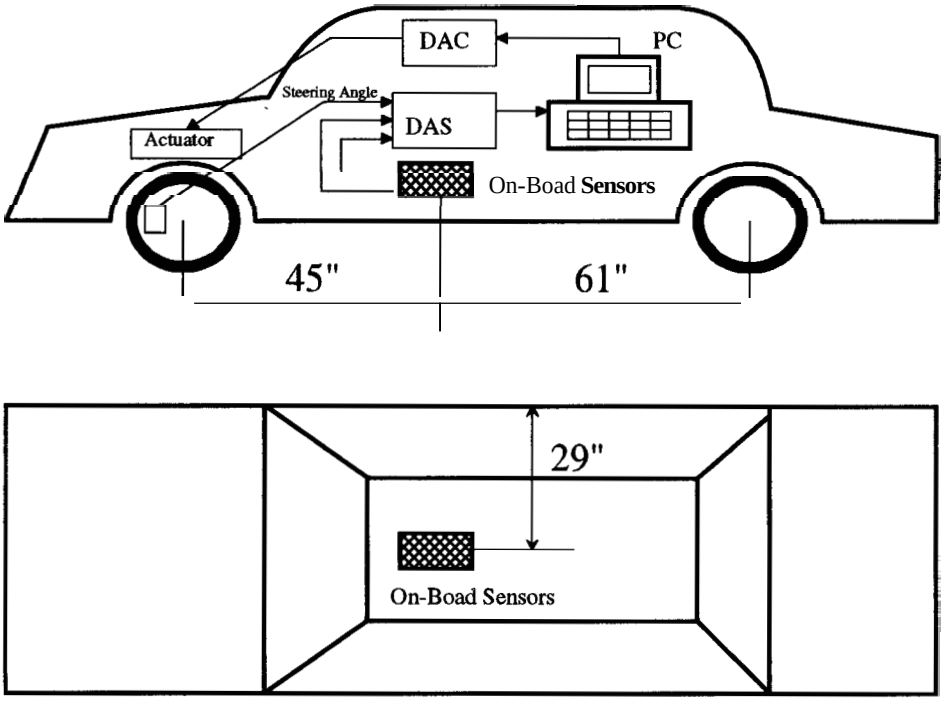

Figure 3.4: Experimental Vehicle

Figure **3.5** shows the representative experimental results. In this experiment, the lane width was $2m$, and the vehicle speed was maintained at $\mathbf{4.44}m/sec$ (10 MPH) by a

human driver. The parameters of the VDT were a_{max}= 0.05g and J_{max}= 0.1g/sec. The uppermost plot shows the accelerometer output, the estimated acceleration, and the simulation result.

Notice that the lateral acceleration measurement is noisy and has a time-varying bias component. The middle plot shows the yaw rate. The lowermost plot shows the steering angle. In this plot, the solid line is the command to the steering actuator, and the dotted line is the actual steering angle measured at the front wheel.

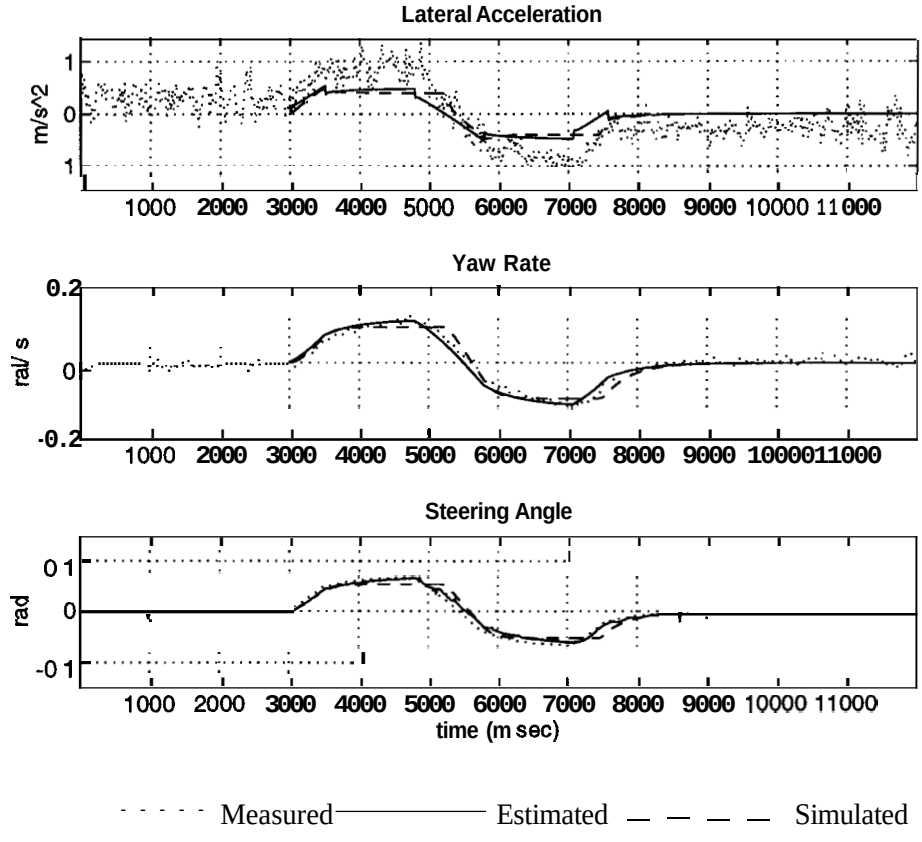

Figure 3.5: Comparison of Measurement and Estimation

Figure **3.6** shows the comparison between the estimated states and the simulated states. The actual states were not measured in this experiment. From these two figures, we can confii a good correspondence between experiment and simulation, which

supports the effectiveness of the proposed estimation scheme, as well as the control scheme.

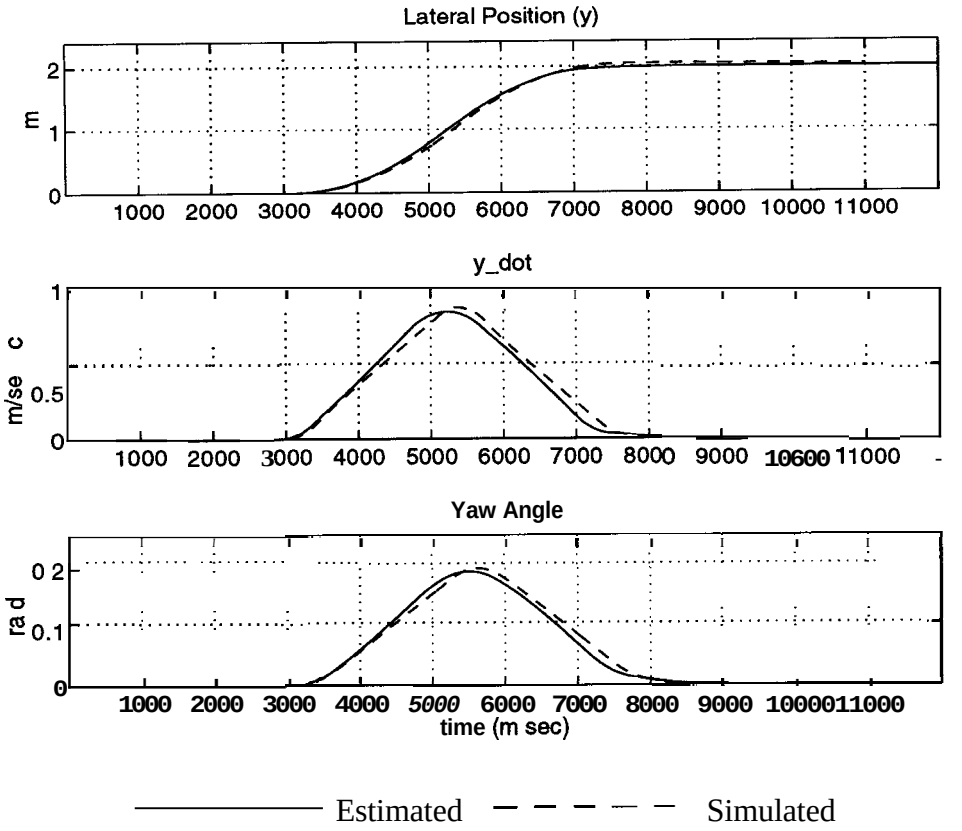

Figure 3.6: Comparison of Estimation and Simulation

3.5 Derivation of Uncertainty Bounds

Each coefficient in equations **(3.6)** and **(3.7)** can be written in terms of the uncertainties in cornering stiffness, mass, and moment of inertia.

$$A_1 = \frac{-4C_s}{\mathbf{m}} = -4\,\frac{\hat{C}_s\left(1+\Delta C_s\right)}{\hat{m}(1+\Delta m)} = \hat{A}_1\left(1+\Delta A_1\right) \qquad \textbf{(3.34)}$$

$$\left.\begin{aligned} \hat{A}_1 &= \frac{-4\hat{C}_s}{\hat{m}} \\ 1+\Delta A_1 &= \frac{(1+\Delta C_s)}{(1+\Delta m)} \end{aligned}\right\} \tag{3.35}$$

where $\hat{C}_s$ and $\hat{m}$ are nominal values given in Table 2.1. ΔC_s and Δm are the uncertainties in parameters. In the same way, other coefficients are written as follows.

$$\left.\begin{aligned} \hat{A}_2 &= 2(l_2 - l_1)\frac{\hat{C}_s}{\hat{m}} \\ 1+\Delta A_2 &= \frac{(1+\Delta C_s)}{(1+\Delta m)} \end{aligned}\right\} \tag{3.36}$$

$$\left.\begin{aligned} \hat{A}_3 &= 2(l_2 - l_1)\frac{\hat{C}_s}{\hat{I}_z} \\ 1+\Delta A_3 &= \frac{(1+\Delta C_s)}{(1+\Delta I_z)} \end{aligned}\right\} \tag{3.37}$$

$$\left.\begin{aligned} \hat{A}_4 &= -2(l_1^2 + l_2^2)\frac{\hat{C}_s}{\hat{I}_z} \\ 1+\Delta A_4 &= \frac{(1+\Delta C_s)}{(1+\Delta I_z)} \end{aligned}\right\} \tag{3.38}$$

As shown above, uncertainties for A_i's , ΔA_i, are in the same form. Recalling the ranges of $\Delta C_s, \Delta m, \Delta I_z$ defined in Table 3.1, we find that

$$|\Delta A_i| \le \max\left(\left|\frac{(1+\Delta C_s)}{(1+\Delta I_z)} - 1\right|\right) = \max\left(\left|\frac{(1+\Delta C_s)}{(1+\Delta m)} - 1\right|\right) = \alpha \tag{3.39}$$

Considering the actual values of $\Delta C_s, \Delta m, \Delta I_z$, we can obtain $0.1739 \le \frac{1+\Delta C_s}{1+\Delta m} \le 1.1764$. From this, we obtain $\alpha = 0.8261$.

For B_i's,

$$B_1 = \frac{2\hat{C}_s}{\hat{m}} \cdot \frac{(1+\Delta C_s)}{(1+\Delta m)} = \hat{B}_1(1+\Delta B_1) \tag{3.40}$$

$$\left.\begin{aligned} \hat{B}_1 &= \frac{2\hat{C}_s}{\hat{m}} \\ 1+\Delta B_1 &= \frac{(1+\Delta C_s)}{(1+\Delta m)} \end{aligned}\right| \tag{3.41}$$

and

$$B_2 = \frac{2\hat{C}_s l_1}{\hat{m}} \cdot \frac{(1+\Delta C_s)}{(1+\Delta m)} = \hat{B}_2(1+\Delta B_2) \tag{3.42}$$

$$\left.\begin{aligned} \hat{B}_2 &= \frac{2\hat{C}_s l_1}{\hat{m}} \\ 1+\Delta B_2 &= \frac{(1+\Delta C_s)}{(1+\Delta m)} \end{aligned}\right\} \tag{3.43}$$

Thus, from **(3.39)**, we obtain

$$|\Delta B_1| \le a, \text{ and } |\Delta B_2| \le a. \tag{3.44}$$

Equations **(3.39)** and **(3.44)** imply that $|\Delta A_i|$ and $|\Delta B_i|$ can be bounded by the same constant.

3.6 Convergence of Tracking Error On Sliding Surface

On the sliding surface defined by **(3.12)**, the filtered error satisfies

$$v = (c_1 t + c_2) \cdot e^{-\lambda t} \tag{3.45}$$

where c_1 and c_2 are some constants, which are dependent on the initial condition of v.

Equation **(3.45)** confirms that the filtered signal (v) as well as its first time derivative exponentially converges to zero on the sliding surface. Therefore, from equation **(3.13)**, we obtain

$$\lim_{t\to\infty} e(t) = 0. \tag{3.46}$$

If we assume that the steering angle remains small,

$$\dot{y}_r \approx V \cdot \varepsilon \tag{3.47}$$

which can be also applied to the relation between y, and $E_{,}$ we obtain the following equation from equations **(3.12)** and **(3.46).**

$$y_r - y_d + \varpi \frac{(\dot{y}_r - \dot{y}_d)}{V} = 0 \tag{3.48}$$

The solution of (3.48), $(y_r - y_d) = (y_r - y_d)\big|_{t=0} \cdot e^{-\frac{V}{\varpi}t}$, confirms that the lateral position error converges to zero exponentially.

$$\lim_{t\to\infty}(y_{,} - y_{,}) = 0 \tag{3.49}$$

With (3.46) and **(3.49),** we finally confirm the convergence of the yaw angle error.

$$\lim_{t\to\infty}(\varepsilon - \varepsilon_d) = 0 \tag{3.50}$$

3.7 Derivation of Control Input

By differentiating **(3.12)** with respect to time, we obtain

$$\mathbf{S} = \ddot{v} + 2\lambda\ddot{v} + \lambda^2\dot{v}. \tag{3.51}$$

Derivatives of *v(t)* are obtained as

$$\dot{v}(t) = (\ln\gamma)\cdot v(t) + e(t) \tag{3.52}$$

$$\begin{aligned}\ddot{v}(t) &= \frac{d}{dt}\dot{v}(t) \\ &= (\ln\gamma)^2 v(t) + (\ln\gamma)\cdot e(t) + \dot{e}(t)\end{aligned} \tag{3.53}$$

$$\begin{aligned}\dddot{v}(t) &= \frac{d}{dt}\ddot{v}(t) \\ &= (\ln\gamma)^3 v(t) + (\ln\gamma)^2 e(t) + (\ln y)\cdot\dot{e}(t) + \ddot{e}(t)\end{aligned} \tag{3.54}$$

Therefore, $S(t)$ and $\dot{S}(t)$ are written **as**

$$S = (\lambda + \ln\gamma)^2 v + (2\lambda + \ln\gamma)e + \dot{e} \tag{3.55}$$

$$\dot{S} = \ln\gamma\cdot(\lambda + \ln\gamma)^2 v + (\lambda + \ln\gamma)^2 e + (2\lambda + \ln\gamma)\dot{e} + \ddot{e}. \tag{3.56}$$

Substituting equation **(3.11)** into equation **(3.56),** we obtain

$$\begin{aligned}\dot{S} &= \ln\gamma\cdot\left(\lambda+\ln\gamma\right)^2 v+\left(\lambda+\ln\gamma\right)^2 e+\left(2\lambda+\ln\gamma\right)\dot{e}+\ddot{e}\\ &=\left(\frac{A_1+A_3}{V}\right)\dot{y}_r-\left(A_1+A_3\right)\varepsilon+\left(\frac{A_2+A_4}{V}\right)\dot{\varepsilon}-\frac{K_y}{m}\left(V_{wy}+\dot{y}_r-V\varepsilon\right)\left|V_{wy}+\mathrm{y},-V\varepsilon\right| \qquad (3.57)\\ &+\left(B_1+B_2\right)\delta-\ddot{y}_d-\ddot{\varepsilon}_d+\left(2\lambda+\ln\gamma\right)\dot{e}+\left(\lambda+\ln\gamma\right)^2 e+\ln\gamma\cdot\left(\lambda+\ln\gamma\right)^2 v\end{aligned}$$

Now, substitute the nominal conditions, i.e. the nominal parameter values and $V_{wy}=0$, in the right hand side of equation (3.57), and equate it to $-K\cdot\mathrm{sgn}(S)$: i.e.,

$$\begin{aligned}&\left(\frac{\hat{A}_1+\hat{A}_3}{V}\right)\dot{y}_r-\left(\hat{A}_1+\hat{A}_3\right)\varepsilon+\left(\frac{\hat{A}_2+\hat{A}_4}{V}\right)\dot{\varepsilon}-\frac{K_y}{m}\left(\dot{y}_r-V\varepsilon\right)\left|\dot{y}_r-V\varepsilon\right|\\ &+\left(\hat{B}_1+\hat{B}_2\right)\delta-\ddot{y}_d-\ddot{\varepsilon}_d+\left(2\lambda+\ln\gamma\right)\dot{e}(t)+\left(\lambda+\ln\gamma\right)^2 e(t)+\ln\gamma\cdot\left(\lambda+\ln\gamma\right)^2 v(t) \qquad (3.58)\\ &=-K\cdot\mathrm{sgn}(S)\end{aligned}$$

where K is called the robustness term, which will cancel all the uncertain dynamics in the control system. This term will be determined later.

From equation (3.58), the control input δ is determined as

$$\delta=\frac{1}{\hat{B}_1+\hat{B}_2}\left\{\begin{array}{l}-\dfrac{\left(\hat{A}_1+\hat{A}_3\right)}{V}\dot{y}_r+\left(\hat{A}_1+\hat{A}_3\right)\varepsilon-\dfrac{\left(\hat{A}_2+\hat{A}_4\right)}{V}\dot{\varepsilon}+\dfrac{K_y}{\hat{m}}\left(\dot{y}_r-V\varepsilon\right)\left|\dot{y}_r-V\varepsilon\right|+\ddot{y}_d+\ddot{\varepsilon}_d\\ -\left(2\lambda+\ln\gamma\right)\dot{e}-\left(\lambda+\ln\gamma\right)^2 e-\ln\gamma\cdot\left(\lambda+\ln\gamma\right)^2 v-K\cdot\mathrm{sgn}(S)\end{array}\right\} \qquad (3.59)$$

The sliding surface $\mathbf{S}=0$ is attractive, if the right hand side of equation (3.57) is bounded by $-\eta\cdot sgn(S)$. With the control input δ of equation (3.59), we have

$$\begin{aligned}\dot{S} &= \frac{\left(\hat{A}_1\Delta A_1+\hat{A}_3\Delta A_3\right)}{V}\mathrm{y}-\left(\hat{A}_1\Delta A_1+\hat{A}_3\Delta A_3\right)\varepsilon+\frac{\left(\hat{A}_2\Delta A_2+\hat{A}_4\Delta A_4\right)}{V}\dot{\varepsilon}\\ &-\frac{K_y}{m}\left[\left(V_{wy}+\mathrm{y}_r-V\varepsilon\right)\left|V_{wy}+\dot{y}_r-V\varepsilon\right|-\left(\dot{y}_r-V\varepsilon\right)\left|\dot{y}_r-V\varepsilon\right|\right]-K\cdot\mathrm{sgn}(S)\\ &+\frac{\left(\hat{\mathrm{B}}_1\Delta B_1+\hat{\mathrm{B}}_2\Delta B_2\right)}{\left(\hat{\mathrm{B}}_1+\hat{\mathrm{B}}_2\right)}\left\{\begin{array}{l}-\dfrac{\left(\dot{A}_1+\dot{A}_3\right)}{V}\dot{y}_r+\left(\hat{A}_1+\hat{A}_3\right)\varepsilon-\dfrac{\left(\dot{A}_2+\dot{A}_4\right)}{V}\dot{\varepsilon}+\dfrac{K_y}{\hat{m}}\left(\dot{y}_r-V\varepsilon\right)\left|\dot{y}_r-V\varepsilon\right|\\ +\ddot{y}_d+\ddot{\varepsilon}_d-\left(2\lambda+\ln\gamma\right)\dot{e}-\left(\lambda+\ln\gamma\right)^2 e-\ln\gamma\cdot\left(\lambda+\ln\gamma\right)^2 v\\ -K\cdot\mathrm{sgn}(S)\end{array}\right\} \qquad (3.60)\\ &\le -\eta\cdot\mathrm{sgn}(S)\end{aligned}$$

which assures the stability of the system.

In this inequality, as η becomes larger, S converges to zero faster. Thus, we can adjust the controller performance by choosing η appropriately.

To check the validity of the inequality, we first consider the following inequality.

$$\begin{aligned}
&(V_{wy} + \dot{y}_r - V\varepsilon)\left|V_{wy} + \dot{y}_r - V\varepsilon\right| - (\dot{y}_r - V\varepsilon)\left|\dot{y}_r - V\varepsilon\right| \\
&\le (V_{wy} + \dot{y}_r - V\varepsilon)\left\{\left|V_{wy}\right| + \left|\dot{y}_r - V\varepsilon\right|\right\} - (\dot{y}_r - V\varepsilon)\left|\dot{y}_r - V\varepsilon\right| \\
&\le V_{wy}\left|V_{wy}\right| + 2\left|V_{wy}\right| \cdot \left|\dot{y}_r - V\varepsilon\right| \\
&\le V_{wm}{}^2 + 2V_{wm} \cdot \left|\dot{y}_r - V\varepsilon\right| \quad , \quad V_{wm} = \max\left(\left|V_{wy}\right|\right)
\end{aligned} \tag{3.61}$$

This inequality represents the bounds for the lateral wind force.

This inequality is combined with other bounds for uncertainties that are derived in Section *3.5* to yield

$$\begin{aligned}
K \ge \eta &+ 2\alpha\left|\frac{\left(\hat{A}_1 + \hat{A}_3\right)}{V}\mathbf{y}, - \left(\hat{A}_1 + \hat{A}_3\right)\varepsilon + \frac{(A2 + \hat{A}_4)}{V}\dot{\varepsilon}\right| \\
&+ \frac{K_y}{\hat{m}}\left\{V^2{}_{wm} + \left[2V_{wm} + \alpha\left|\dot{y}_r - V\varepsilon\right|\right]\left|\dot{y}_r - V\varepsilon\right|\right\} \\
&+ \alpha\left|\ddot{y}_d + \ddot{\varepsilon}_d - (2\lambda + \ln\gamma)\dot{e} - (\lambda + \ln\gamma)^2 e - \ln\gamma(\lambda + \ln\gamma)^2 v\right|
\end{aligned} \tag{3.62}$$

The robustness term K *in* equation *(3.59)* must satisfy equation *(3.62).*

3.8 Derivation of Bounds For γ

3.8.1 Upper Bound

The gain crossover frequency of the filter is obtained from equation *(3.13)* as

$$\omega_{g.c.} = \sqrt{1 - (\ln\gamma)^2} \tag{3.63}$$

Then, the upper bound for γ is obtained by c o n f i i g the gain crossover frequency of the filter to less than the given frequency, Ω_l .

$$\sqrt{1-(\ln\gamma)^2} \le \Omega_l \tag{3.64}$$

This inequality can be also written as

$$\gamma \le e^{-\sqrt{1-\Omega_l^2}} \tag{3.65}$$

In the application to lane change maneuvers, Ω_l is selected as the upper limit of the human-sensitive frequency range.

3.8.2 Lower Bound

With the condition **(3.16),** the steady state filtered error for the worst case becomes

$$v_{ss} = \frac{\Phi}{\lambda^2}. \tag{3.66}$$

where, Φ is the boundary thickness when the saturation function **(3.19)** is used in the control law **(3.17).** Using the balance condition introduced in **[34],** we can relate the robust term and the boundary thickness as

$$K\left(y_d, \dot{y}_d, \varepsilon_d, \dot{\varepsilon}_d\right) = \lambda \cdot \Phi \tag{3.67}$$

To simplify the analysis, λ is chosen as follows.

$$\lambda = \frac{\max\left(K\left(y_d, \dot{y}_d, \varepsilon_d, \dot{\varepsilon}_d\right)\right)}{\Phi} \tag{3.68}$$

With this choice of λ ,the boundary layer thickness is constant.

Then, **(3.66)** is written **as**

$$v_{ss} = \frac{K_{\max}}{\lambda^3} \tag{3.69}$$

where, $K_{\max} = \max\left(K\left(y_d, \dot{y}_d, \varepsilon_d, \dot{\varepsilon}_d\right)\right)$.

From **(3.69),** the steady state tracking error **is** derived as

$$e_{ss}^{v} = -\ln\gamma \cdot \frac{K_{max}}{\lambda^3} . \quad \textbf{(3.70)}$$

Now, denoting the allowable steady state tracking error as ζ, we can place the upper bound on e_{ss}^{v} as

$$-\ln\gamma \cdot \frac{K_{max}}{\lambda^3} \leq \zeta \quad \textbf{(3.71)}$$

From (3.71), the lower bound for ybecomes

$$y \geq e^{-\frac{\lambda^3}{K_{max}}\cdot\zeta} . \quad \textbf{(3.72)}$$

3.9 Summary

In this chapter, we investigated the lane change maneuvers as a tracking control problem with the VDT. The bicycle model was modified to represent the lateral position with respect to the center of the lane where the lane change would begin. The sliding mode control algorithm was studied as the control algorithm. The sliding surface was constructed with the filtered error to achieve smooth control action. The sliding mode controller with an error filter was proposed to achieve acceptable comfort level and steady state error.

The reduced order Kalman filter based on the linear model was designed as the state estimation algorithm, and found to provide satisfactory state estimates from experimental results.

Experimental results confirmed that the combination of the sliding mode controller and the state estimator was effective for lane change maneuvers at low speeds. Even though high speed tests were not performed, similar results can be expected because the response of a vehicle resembles the bicycle model more at higher speeds.

Chapter 4

Unified Lateral Guidance with Road-Reference System and On-Board Sensor

In this chapter, a unified control system structure for both lane change and lane following maneuvers including transition maneuvers between the two types of maneuvers will be presented. The sensing system includes the road reference sensing systems proposed by PATH program and yaw rate sensor. Thus, the magnets embedded in the road and two magnetometers installed on the vehicle constitute the road reference sensing system.

4.1 Control System Structure

Previously, switching between the two different controllers for the lane change maneuvers and the lane following maneuvers was studied in [5]. Since the two controllers involved in this switching were dynamic controllers, the switching method had a problem in setting the initial conditions for the controllers. Thus, the transition response during the switching shows large acceleration even though large jerk response could be avoided. In addition, the lateral position estimation during the lane change maneuvers, which involves integrals with uncertain initial conditions, was necessary because the lane change control was attempted as a tracking control.

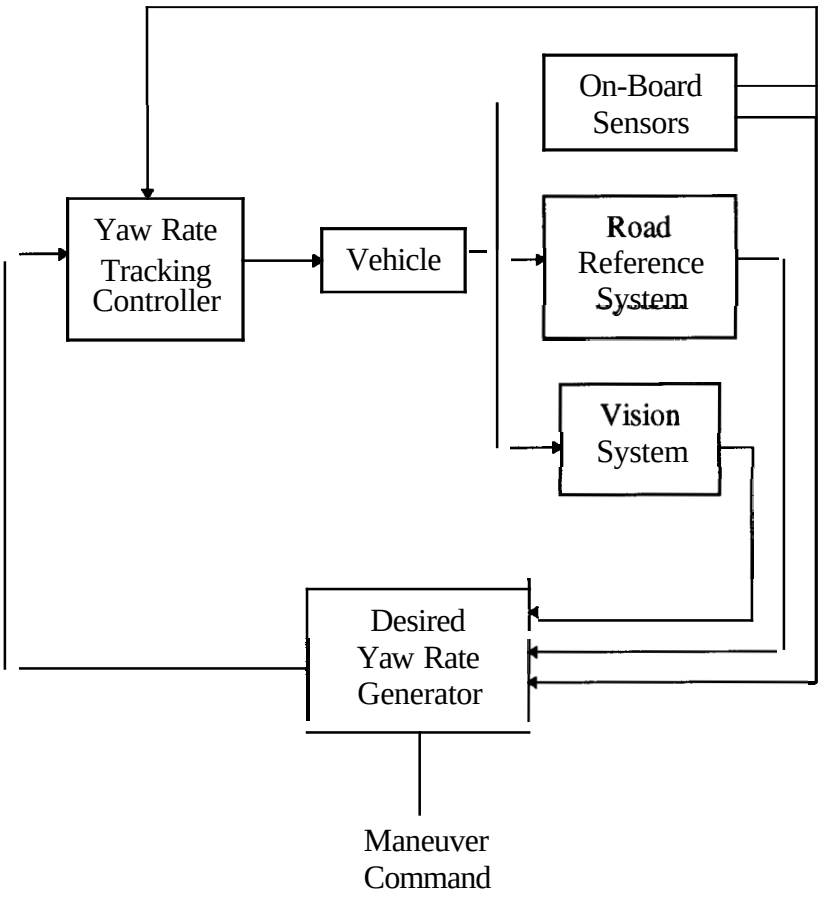

Figure 4.1: Structure of Unified Lateral Control System

In order to avoid these problems, the unified lateral control system is proposed as shown in Figure **4.1.** This system is in cascade structure, which can be seen in the previous literature([3][23]). Pappas and Kyriakopoulos proposed a cascade control algorithm for guiding a vehicle-like robot considering the nonholonomic constraint of the vehicle dynamics[23]. Since the vehicle-like robot runs at very low speed, the effect of side slip of a vehicle, which is evident when a vehicle runs at high speed, is not considered in [23]. Thus, the unicycle model is used for the dynamics of the vehicular object. The stability of the whole system has been achieved by placing high gain at the yaw rate tracking error, and is proven via the singular perturbation theory. This high gain applied to the yaw rate tracking error is potentially undesirable in vehicle lateral control applications since the ride comfort is one of the key issues. Ackermann et. al.[3] proposed

the same structure control algorithm for the vehicle lateral control. In this algorithm, a simple bicycle model is used to include the effect of side slip of a vehicle. For the yaw rate tracking controller, they proposed a sliding mode controller. To eliminate the chattering effect of the sliding controller, they adopted the equivalent control method for the discrete sliding mode systems based on Filippov's construction of equivalent dynamics in sliding mode, which result in a linear output feedback controller ([34][35]). Although they showed the stability of each block in the system, they do not prove the stability of the whole system.

Here, the cascade structure control system is extensively exploited in order to include multiple maneuvers, which include lane change and lane following maneuvers. All the sensor data are provided to the desired yaw rate generator, where the desired yaw rate for each maneuver is generated, while data from the on-board sensors are provided to the yaw rate tracking controller. The rationale of this strategy of using sensor data is due to the limited availability of the magnetic sensor outputs, which are available only during the lane following maneuvers. Thus, lane change maneuvers are performed in open loop manner in the sense that the position measurement is not available. To avoid performing the lane change maneuvers completely in open loop manner, the desired trajectory information is expressed in terms of the yaw rate. By tracking the yaw rate, we can achieve the lane change maneuvers as in the closed loop manner because the tracking error of the yaw rate reflects the motion error for the desired maneuvers.

Lane following maneuvers are achieved by deciding the yaw rate from the analysis of the kinematics of the lateral position measurement. This analysis of the kinematics is totally dependent on the measurement system. Thus, the scheme can incorporate other lateral position measurement systems, such as vision sensor, with the same yaw rate tracking controller. With this methodology, we can achieve various maneuvers with various lateral position measurement systems in some unified way: i.e. the desired maneuvers are achieved by kinematics analysis and the yaw rate tracking controller design. Therefore, we call this methodology the unified lateral guidance algorithm.

4.2 Yaw Rate Tracking Controller Design

Once the desired yaw rate for a desired maneuver is decided, the unified lateral control system needs a controller to follow the desired yaw rate. Here, we design a controller utilizing only the yaw rate sensor output to track the desired yaw rate. Since the system order of the simplified vehicle model is two and only one sensor is used to measure one of the system state, we need an observer for the unmeasured state, V_y .

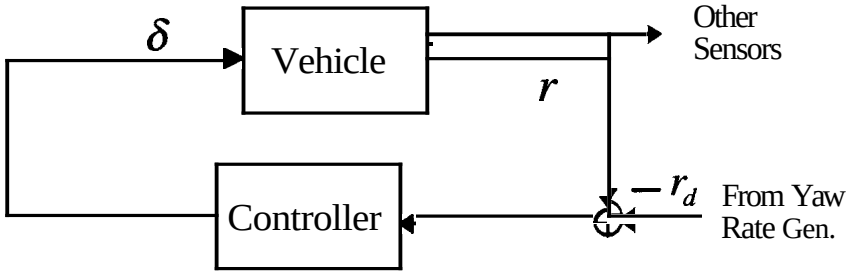

Figure 4.2: Yaw Rate Tracking Controller

The controller in Figure **4.2** is designed via the Lyapunov-based scheme[30]. The Lyapunov-based control scheme is advantageous in proving the stability of the overall feedback system, which is in cascade structure. The controller is designed with respect to the nominal road condition, but the controller gains are scheduled with respect to the longitudinal speed of the vehicle since this is the primary parameter affecting vehicle response as mentioned in [11]. In addition, the road condition cannot be measured and is very difficult to estimate whereas the longitudinal vehicle speed can be reliably measured.

4.2.1 Vehicle Model Description for Yaw Rate Controller Design

For the design of the yaw rate tracking control, the bicycle model is used. However, it is expressed as follows in order to congregate the totally uncertain quantities in the expression, such as cornering stiffness, mass, and moment of inertia of a vehicle.

$$\dot{r} = \left(a_1 r + a_2 V_y + b_1 \delta\right) I_c \tag{4.1}$$

$$\dot{V}_y = \left(a_3 r + a_4 V_y + b_2 \delta\right) m_c - V_x r \tag{4.2}$$

Here, the coefficients are defined as follows.

$$a_1 = -2\frac{l_1^2 + l_2^2}{V_x},\ a_2 = -2\frac{l_1 - l_2}{V_x},\ a_3 = -2\frac{l_1 - l_2}{V_x},\ a_4 = -\frac{4}{V_x} \tag{4.3}$$

$$b_1 = 2l_1,\ b_2 = 2 \tag{4.4}$$

$$I_c = \frac{C_s}{I_z},\ m_c = \frac{C_s}{m} \tag{4.5}$$

The symbols in the above equations are listed in Table 2.1.

In this model, the input of the vehicle is the front wheel steering angle (δ). Unlike the approach in Chapter 3, only the yaw rate (r) is measured as an output of the vehicle. Thus, the lateral velocity is taken as an internal state, and an estimation algorithm for the lateral velocity is designed. It is assumed that the longitudinal velocity can be measured from wheel speed.

4.2.2 Design of Yaw Rate Tracking: Controller

The yaw rate controller is designed via Lyapunov method. One of the advantages of this design methodology is that the controller can be expressed analytically in terms of the known quantities and longitudinal velocity. In the following design, it is assumed that desired yaw rate $\left(r_d\right)$ is smooth and the magnitude of its time derivative $\left(\dot{r}_d\right)$ is bounded.

An output feedback controller is proposed by the following theorem.

Theorem 4.1: Yaw Rate Tracking Controller

Consider the model of a vehicle represented as (4.2) and (4.1). Assume that the yaw rate (r) and the longitudinal velocity (V_x) are measured. Assume that desired yaw rate (r_d) is smooth and the magnitude of its time derivative $(\dot{r}_d)$ is bounded. Then, with the following dynamic output feedback controller

$$\dot{\hat{V}}_y = -\left(2m_c\frac{(l_1-l_2)}{V_x}+V_x\right)r-4\frac{m_c}{V_x}\hat{V}_y+2m_c\delta-2\frac{(l_1-l_2)}{V_x}I_c(r-r_d)d_0 \tag{4.6}$$

$$\delta=\frac{1}{2l_1}\left(2\frac{(l_1^2+l_2^2)}{V_x}r+2\frac{(l_1-l_2)}{V_x}\hat{V}_y+\frac{\dot{r}_d}{I_c}-\lambda_e(r-r_d)\right) \tag{4.7}$$

we can achieve

$$r(t)\to r_d(t),\quad \hat{V}_y(t)\to V_y(t)\quad \text{as}\quad t\to\infty,$$

and the magnitude of V_y is bounded.

Here, $\hat{V}_y$ denotes estimate of the lateral velocity and λ_e is a positive constant that represents the yaw rate convergence rate. The relative weight on estimation error with respect to the yaw rate tracking error is defined as a positive constant d_0.

(Proof)

Define the following two quantities for notational convenience.

$$\text{e, } = r-r_d \tag{4.8}$$

$$\tilde{V}_y = V_y-\hat{V}_y \tag{4.9}$$

Equation (4.8) denotes the yaw rate tracking error, and equation (4.9) denotes the estimation error.

Consider the estimation of the lateral velocity in the following form.

$$\dot{\hat{V}}_y=\left(a_3r+a_4\hat{V}_y+b_2\delta\right)m_c-V_xr+\chi \tag{4.10}$$

Here, χ will be determined later, and a_i's and b_i's are defined in (4.3) and (4.4), respectively.

Then, the dynamics for $\tilde{V}_y$ can be obtained as follows.

$$\dot{\tilde{V}}_y = a_4 \tilde{V}_y m_c - \dot{\chi} \tag{4.11}$$

Now consider the following control Lyapunov function candidate.

$$V_1 = \frac{1}{2} e_r^2 + \frac{1}{2d_0} \tilde{V}_y^2 \tag{4.12}$$

Differentiating **(4.12)** with respect to time, and considering **(4.1)** and **(4.10),** we can obtain

$$\dot{V}_1 = e_r \left\{ \left(a_1 r + a_2 \hat{V}_y + b_1 \delta \right) I_c - \dot{r}_d \right\} + \tilde{V}_y \left(a_2 I_c e_r - \frac{\dot{\chi}}{d_0} \right) + a_4 \frac{m_c}{d_0} \tilde{V}_y^2 . \tag{4.13}$$

Now take $\chi = d_0 I_c a_2 e_r$ and δ as in **(4.7).** Then, we have

$$\dot{V}_1 \le -\lambda_e e_r^2 - 4 \frac{m_c}{V_x d_0} \tilde{V}_y^2 = -W_1 \left(e_r, \tilde{V}_y \right) \tag{4.14}$$

By applying Theorem **A.5,** we can confirm the global uniform stability of the system shown in Figure **4.2.**

By applying Theorem **A.7** with V_1 and W_1, we finally obtain

$$r(t) \to r_d(t), \quad \hat{V}_y(t) \to V_y(t) \quad \text{as} \quad t \to \infty .$$

Boundedness of the lateral velocity can be shown as follows.

Now replace δ in equation **(4.2)** with **(4.7).** Then, **(4.2)** becomes

$$\dot{V}_y = \left(a_4 - \frac{a_2 b_2}{b_1} \right) V_y + \left(a_3 - \frac{a_1 b_2}{b_1} \right) r + \frac{a_2 b_2}{b_1} \tilde{V}_y - \frac{b_2}{b_1} \frac{\lambda_e}{I_c} e_r + \frac{b_2}{b_1} \frac{\dot{r}_d}{I_c} . \tag{4.15}$$

By considering the definition of a_i's, we can find that

$$\left(a_4 - \frac{a_2 b_2}{b_1} \right) = -\frac{4}{V_x} + \frac{1}{2} \left(l_1 - \frac{1}{l_1} \right) . \tag{4.16}$$

From the typical values listed in Table **2.1,** we can show that

$$\left(a_4 - \frac{a_2 b_2}{b_1} \right) < 0 \tag{4.17}$$

Thus, the dynamics of V_y is stable. Therefore, the magnitude of V_y is bounded if r, $\tilde{V}_y$, e_r, and $\dot{r}_d$ are bounded. Since $e_r \to 0$ as $t \to \infty$, $r \to r_d$ as $t \to \infty$. In addition,

$\tilde{V}_y \to 0$ as $t \to \infty$. Therefore, the magnitude of V_y is bounded if r_d and $\dot{r}_d$ are bounded. From the assumptions on r_d and $\dot{r}_d$, we can conclude that the magnitude of V_y is bounded. ■

4.3 Desired Yaw Rate for Lane Following Maneuvers with Magnetic Road Reference System

4.3.1 Kinematics Analysis for Lane Following

Lane following maneuver is attempted by forcing the lateral position measured by the magnetic road reference system to converge to zero. To achieve the convergence of the measured lateral position, the kinematics of the measurements has been conducted considering Figure 4.3.

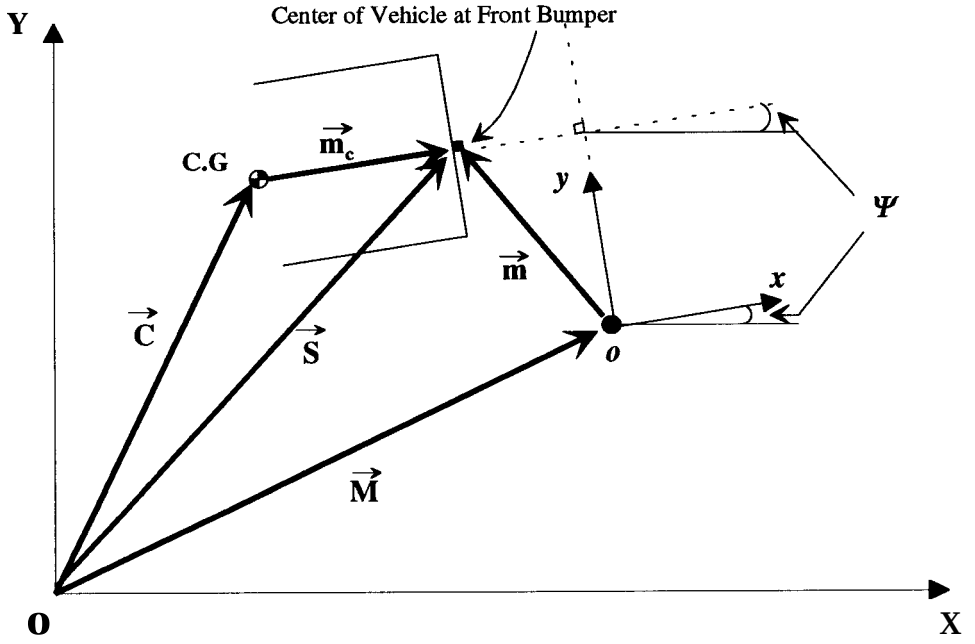

Figure 4.3: Kinematics Analysis for Lateral Position Measurement

First, adopt a coordinate system **OXY** which is fixed in space, and the unit vectors for **OX** and **OY** are represented as **i,** and **i,** , respectively. Let a magnet be located at $(\mathbf{X_M}, \mathbf{Y_M})$ with respect to **OXY,** and the vector **M** denotes the position vector for the magnet. Now, consider a rotating coordinate system ***oxy*** whose origin is fixed at the position of the magnet with the unit vectors **i,** and $\mathbf{i}_y$. Note that the two sets of the unit vectors are related **as** follows.

$$\begin{bmatrix} \mathbf{i}_x \\ \mathbf{i}_y \end{bmatrix} = \begin{bmatrix} cos\Psi & -sin\Psi \\ sin\Psi & cos\Psi \end{bmatrix} \begin{bmatrix} \mathbf{i}_x \\ \mathbf{i}_y \end{bmatrix} \tag{4.18}$$

Here, Ψ is the yaw angle of a vehicle with respect to **OX** axis.

Then, the measured position, **(x,,y,)** , are represented by the vector **m** , and can be written as

$$\mathbf{m} = x_s\mathbf{i}_x + y_s\mathbf{i}_y . \tag{4.19}$$

Considering equation **(4.18),** we can write equation **(4.19)as**

$$\vec{\mathbf{m}} = (\mathbf{x,}\ \mathrm{COSY} - \mathbf{y,}\ \sin\Psi)\mathbf{i}_X + (\mathbf{x,}\ \sin\Psi + \mathbf{y,}\ \cos\Psi)\mathbf{i}_Y . \tag{4.20}$$

From the geometrical relations of the vectors as shown in Figure **4.3,** we have

$$\vec{\mathbf{S}} = \vec{\mathbf{M}} + \vec{\mathbf{m}} \tag{4.21}$$

and

$$\vec{\mathbf{S}} = \vec{\mathbf{C}} + \vec{\mathbf{m}}_c \tag{4.22}$$

where,

$$\vec{\mathbf{C}} = x_c\mathbf{i}_X + y_c\mathbf{i}_Y \tag{4.23}$$

and

$$\vec{\mathbf{m}}, = d, \cos\Psi\mathbf{i}_X + d, \sin\Psi\mathbf{i}_Y . \tag{4.24}$$

It **is** worthwhile to note that the lateral and the longitudinal velocity are related with X, and $\dot{y}_c$ as follows.

$$V_x = \dot{x}_c \cos\Psi + \dot{y}_c \sin\Psi \tag{4.25}$$

$$V_y = \dot{y}_c \cos\Psi - \dot{x}_c \sin\Psi \tag{4.26}$$

From equation **(4.21),** we have

$$\vec{S} = \dot{\vec{m}}$$

since the magnet is fixed in space.

With equation **(4.20),** we obtain

$$\begin{aligned}\vec{S} = \dot{\vec{m}} = &\left\{\dot{x}_s \cos\Psi - \dot{y}_s \sin\Psi - \dot{\Psi}\left(x_s \sin\Psi - y, \cos\Psi\right)\right\}\mathbf{i}_X \\ &+\left\{\dot{x}_s \sin\Psi + \dot{y}_s \cos\Psi + \dot{\Psi}\left(x_s \cos\Psi - y, \sin\Psi\right)\right\}\mathbf{i}_Y \ .\end{aligned} \tag{4.27}$$

From equation **(4.22),** we can get

$$\dot{\vec{S}} = \left(\dot{x}_c - \dot{\Psi} d_s \sin\Psi\right)\mathbf{i}_X + \left(\dot{y}_c + \dot{\Psi} d_s \cos\Psi\right)\mathbf{i}_Y \tag{4.28}$$

By solving equations **(4.27)** and **(4.28)** together, we find

$$\dot{x}_s = \dot{x}_c \cos\Psi + \dot{y}_c \sin\Psi + \Psi y_s \tag{4.29}$$

$$\dot{y}_s = \dot{y}_c \cos\Psi + \dot{\Psi} d_s - \dot{x}_c \sin\Psi - \dot{\Psi} x_s \ . \tag{4.30}$$

Recalling **(4.25)** and **(4.26),** we can write **(4.29)** and **(4.30)** as follows.

$$\dot{x}_s = V_x + \Psi y_s \tag{4.31}$$

$$\dot{y}_s = V_y + \dot{\Psi}\left(d_s - x_s\right) \tag{4.32}$$

Equations **(4.31)** and **(4.32)** represent time derivative of the longitudinal and the lateral position measurement, respectively. From **(4.32),** it is possible to make the lateral position measurement converge to zero by posing the desired dynamics of the lateral position measurement as $\dot{y}_s = -\lambda_s y_s$.

4.3.2 Desired Yaw Rate for Lane Following Maneuver

Once the desired dynamics of the lateral position measurement is obtained, it can be expressed in terms of the yaw rate **(4.32).** This yaw rate is the desired yaw of the vehicle to be realized by the yaw rate tracking controller designed in Section **4.3.** The yaw rate of the vehicle that ensures the desired dynamics of the lateral position measurement, $\dot{y}_s = -\lambda_s y_s$, is achieved by the following theorem.

Theorem 4.2: Desired Yaw Rate for Lane Following Maneuver

Assume that the longitudinal position(x,) and the lateral position(y,) of the vehicle are available continuously. Then, the desired yaw rate(r_d) to make y, converge to zero can be obtained as

$$r_d = -\left(\frac{V_y + \lambda_s y_s}{d_s - x_s}\right) \tag{4.33}$$

(Proof)

Take the Lyapunov function candidate as

$$V_s = \frac{1}{2} y_s^2 . \tag{4.34}$$

Then, the time derivative becomes as follows considering **(4.32).**

$$\dot{V}_s = y_s\left(V_y + r\left(d_s - x_s\right)\right) \tag{4.35}$$

By taking r as **(4.33),** we can write **(4.35)** as follows.

$$v, = -\lambda_s y_s^2 \tag{4.36}$$

By applying Theorem **A.7,** we can achieve y, $\rightarrow 0$ as $t \rightarrow \infty$. ■

Remark:

The desired yaw rate as shown in **(4.33)** results in the dynamics for the lateral position measurement as

$$\dot{y}_s = -\lambda_s y_s . \tag{4.37}$$

Thus, the larger λ_s is, the faster the convergence of y_s is. However, the resulting acceleration becomes larger as A, becomes larger. Since one of our goals of the lateral guidance is to maintain passengers' ride comfort during the guidance, we cannot make λ_s arbitrary large considering the resulting acceleration. Thus, the value of λ_s is decided by compromising the ride comfort and the tracking performance.

4.4 Desired Yaw Rate for Lane Change Maneuver

As mentioned above, the lateral position measurement from the road reference sensing system is available only in the limited range near the magnets. Since the lane change maneuvers under the PATH scenario controls the vehicle to move between two adjacent lanes, the vehicle should pass through the region where the road reference system information is not available. Thus, the control algorithm for lane following maneuvers can not be implemented.

Here, we propose a strategy for the lane change maneuvers as shown in Figure **4.4.** The lane change maneuvers are divided into three stages: transition I, transition II, and the VDT tracking stage. During the VDT tracking stage, the lateral position can not be measured by the road reference sensing system because the vehicle is in the range where the magnetic fields of the magnets are weak. Thus, the VDT information is translated into the desired yaw rate via

$$r_{change} = \frac{\ddot{y}_{VDT}}{V_x}. \tag{4.38}$$

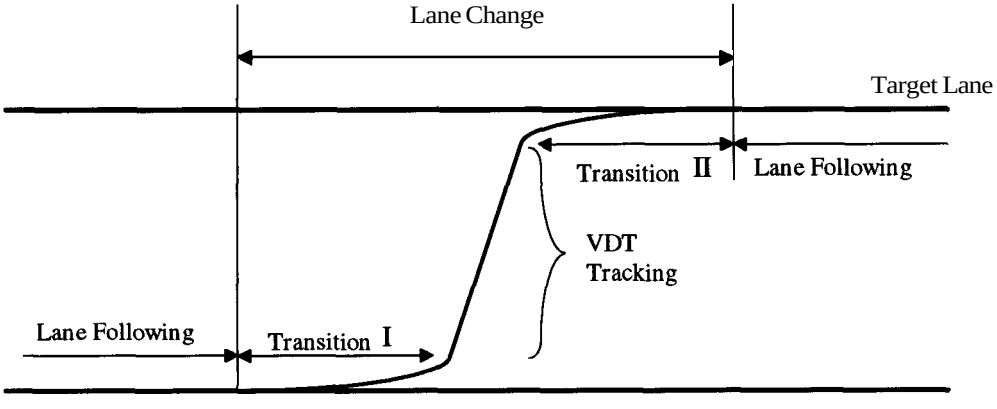

Figure 4.4: Strategy For Lane Change Maneuvers

Transition I stage corresponds to the region that is up to 0.3m apart laterally from the center of the lane where the lane change maneuvers begin. During transition I stage, a

smooth transition from tracking the road reference system to tracking the VDT is attempted by taking the desired yaw rate as follows.

$$r_I = w(t)r_{change} + (1 - w(t))r_{follow} \quad , \quad |w(t)| \le 1 \tag{4.39}$$

The weighting function, $w(t)$, is designed not to produce large lateral jerk of the vehicle during the transition. Here, the following weighting function is used.

$$w(t) = 1 - e^{-\phi(t-t_c)} \tag{4.40}$$

Here, φ represents the smoothness of the convergence of $w(t)$. t denotes the running time of the vehicle system, and t_c represents the start time of the transition I stage.

The transition II stage corresponds to the region that is up to 0.3m apart laterally from the target lane. During the transition II stage, a smoothing transition from VDT tracking to the lane following maneuvers is attempted by the following yaw rate.

$$r_{II} = w(t)r_{change} + (1 - w(t))r_{follow} \quad , \quad |w(t)| \le 1 \tag{4.41}$$

Here, the following weighting function is used.

$$w(t) = e^{-\phi(t-t_c)} \tag{4.42}$$

where, t_c is the start time of the transition II stage. Once $w(t)$ reaches some threshold value, indicating that the vehicle has neared to the target lane, the desired yaw rate is obtained totally from lane following maneuvers.

Like the lane following maneuvers, the desired yaw rate is realized by the yaw rate tracking controller. Thus, we can achieve multiple maneuvers by one feed controller. Therefore, the two maneuvers of the lateral guidance can be realized by the unified methodology.

Remark:

In the previous research [5], two dynamic tracking controllers were designed: One was for the lane change maneuvers and the other for lane following maneuvers. In this case, the switching between the two maneuvers involved setting the initial condition of the controller states because both controllers are dynamic feedback controller. The initial

condition of the controller should be carefully set in order to avoid undesirable transient during the switching. Since the controllers were designed based on vehicle model, the "careful" initial condition setting was not possible with model uncertainties.

4.5 Stability of Overall System

Since each block of Figure **4.1** has been designed separately, the stability of the overall system, and convergence of the tracking error in the case of lane following maneuvers and convergence of the estimation error are not proved. In this section, we prove the stability of the overall system. Since each block is based on the Lyapunov design, the stability of the whole system can be proven by building a Lyapunov candidate for the entire system. This methodology based Lyapunov design is more convenient to prove the stability than the previous sliding mode controller design based on yaw rate tracking structure presented in [3]. There, the stability of the whole system is assumed by presuming that the error dynamics of the estimation are extremely fast.

Theorem 4.3: (Stability and Convergence for Lane Following Maneuver)

With the desired yaw rate,

$$r_d = -\frac{\hat{V}_y - \lambda_s y_s}{d_s - x_s} \tag{4.43}$$

the estimator of lateral velocity **(4.6),** and the yaw rate tracking controller **(4.7),** we can achieve

$$y_s(t) \to 0,\ e_r(t) \to 0, \text{ and } \tilde{V}_y(t) \to 0 \quad \text{as} \quad t \to \infty .$$

if we choose λ_e and λ_s as follows.

$$\lambda_e > \frac{1}{4\lambda_s} \tag{4.44}$$

$$\lambda_s > -\frac{d_0}{4a_4 m_c} \tag{4.45}$$

(Proof)

Take a Lyapunov candidate as

$$V = V_1 + V_s$$

Here, V_1 is defined as (4.12) and V_s as (4.34).

Take the first time derivative of the Lyapunov function considering (4.43).

$$\dot{V} = y_s\left(\hat{V}_y + r_d\left(d_s - x_s\right)\right) + \tilde{V}_y y_s + e_r y_s + \dot{V}_1 \tag{4.46}$$

Now consider (4.6), (4.7), and (4.14). Then, (4.46) becomes

$$\dot{V} \le -\lambda_s y_s^{\,2} + \tilde{V}_y y_s + e_r y_s - \lambda_e e_r^{\,2} + a_4 \frac{m_c}{d_0} \tilde{V}_y^{\,2} \tag{4.47}$$

To proceed further, we need to consider the following equalities.

$$-\lambda_s y_s^{\,2} + e_r y_s = -\lambda_s\left(y_s - \frac{e_r}{2\lambda_s}\right)^2 + \frac{e_r^{\,2}}{4\lambda_s}$$

$$a_4 \frac{m_c}{d_0}\tilde{V}_y^{\,2} + y_s \tilde{V}_y = a_4 \frac{m_c}{d_0}\left(\tilde{V}_y + \frac{d_0}{2a_4 m_c} y_s\right)^2 - \frac{d_0}{4a_4 m_c} y_s^{\,2}$$

Then, (4.47) becomes

$$\dot{V} \le -\left(\lambda_e - \frac{1}{4\lambda_s}\right)e_r^{\,2} - \left(\lambda_s + \frac{d_0}{4a_4 m_c}\right)y_s^{\,2} - \lambda_s\left(y_s - \frac{e_r}{2\lambda_s}\right)^2 + a_4 \frac{m_c}{d_0}\left(\tilde{V}_y + \frac{d_0}{2a_4 m_c} y_s\right)^2$$

If we choose λ_e and λ_s to satisfy (4.44) and (4.45), respectively, then, from Theorem A.5, the stability of the whole systems is proved.

By applying Theorem A.7, we obtain

$$y_s(t) \to 0,\ e_r(t) \to 0, \text{ and } \tilde{V}_y(t) \to 0 \quad \text{as} \quad t \to \infty. \qquad \blacksquare$$

Remarks:

1. Considering the typical values of the vehicle model parameters listed in Table 2.1, (4.45) becomes

$$a_s > 0.0026875 \cdot V_x d_0 . \tag{4.48}$$

2. During lane change maneuvers, the desired yaw rate is decided in open loop manner because the lateral position is not available. Thus, no further stability proof is necessary.

4.6 Simulation Results

To validate the proposed unified lateral guidance algorithm, simulations have been conducted. In the simulation, magnets are modeled as a dipole, and lateral position is obtained from the method introduced in Chapter 2. The spacing of magnets is selected to be 1m. Yaw rate sensor is the on-board sensor. Sensor noises for magnetometers and the yaw rate sensor are modeled as white normal signals whose powers are obtained from experimental data. The complex vehicle model proposed in [26] is used to simulate the vehicle response. Parameters of the VDT are chosen from Figure 2.21: lateral acceleration $= 0.2$g, and lateral jerk $= 0.2$g/sec. According to Figure 2.21, the transition time with theses parameters becomes 3.88 sec.

Convergence parameters, λ_e and λ_s, introduced in (4.7) and (4.33) satisfying (4.44) and (4.48) are decided after choosing $d_0 = 4.0$, which corresponds to 2 times more weight on yaw rate error. With $d_0 = 4.0$, (4.48) becomes

$$a_s > 0.01075 \cdot V_x \tag{4.49}$$

Considering (4.49), λ_s is chosen as

$$\lambda_s = 0.01075 \cdot V_x \kappa_s \tag{4.50}$$

where, κ_s is a constant and $\kappa_s > 1$.

To determine the value of κ_s, we investigate the effect on the vehicle response through simulations when the value of κ_s varies. Simulation results are shown in Figure

4.5 and Figure 4.6. Lines in these two figures represent the system responses for different values of κ_s. Here, the tracking error is defined as the distance between the center of gravity and the road center, and shown in the upper plot of the figures. The lower left plot shows the steering angle variation during the maneuver, and the lower right plot displays the resulting lateral acceleration. Figure 4.5 shows the case when the initial tracking error of the vehicle is $0.3m$. Figure 4.6 shows the results for the $0.1m$ initial tracking error. Considering the tracking error convergence time and the resulting lateral accelerations, we choose $\kappa_s = 5.0$. With $\kappa_s = 5.0$, we can reduce the convergence time to almost a half of the one for $\kappa_s = 3.0$. In addition, we can limit the resulting lateral acceleration by $0.2g$ for the case with a large initial tracking error shown in Figure 4.5.

The nominal performance of the proposed scheme is shown in Figure 4.7 and Figure 4.8. Here, the lane change command is issued at 3 sec, and the initial tracking error is set to be $0.3m$. Until 3 sec, the desired yaw rate is generated using (4.43). After 3 sec and until the lateral position of the vehicle with respect to the center of a lane becomes $0.3m$, the desired yaw rate is generated using (4.39). After the vehicle moves more than $0.3m$ laterally, the desired yaw rate is generated from (4.38). Then, the desired yaw rate is obtained from (4.41) once the vehicle enters the region where the distance from the center of the target lane is less than $0.3m$. After the transition time of the VDT, the desired yaw rate is again obtained from (4.43). In the upper plot of Figure 4.7, the vehicle position with respect to the center of the original lane is presented. The lower left plot shows the steering angle variation during the maneuver and the lower right plot shows the resulting lateral acceleration. With the choice of $\kappa_s = 5.0$, the resulting lateral acceleration can be bounded by $0.2g$ through the maneuver. Figure 4.8 shows the yaw rate tracking performance by displaying the desired yaw rate in the upper plot and the yaw rate error in the lower plot.

Figure 4.9 and Figure 4.10 show the results for the slippery road condition, where the cornering stiffness is reduced to the 30% of the nominal value. From these two figures, we can still achieve a similar tracking performance as the nominal road condition

except for more active steering action. **Thus,** we can verify the robustness of the unified lateral guidance algorithm to system uncertainties.

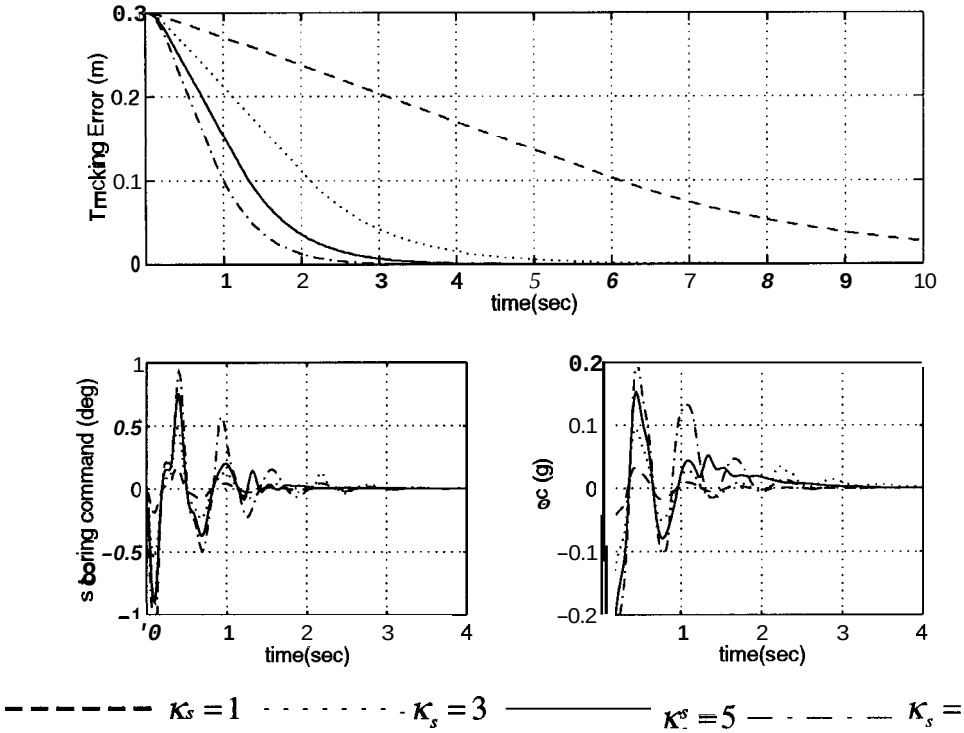

Figure 4.5: Convergence Test (Initial Tracking Error =0.3m)

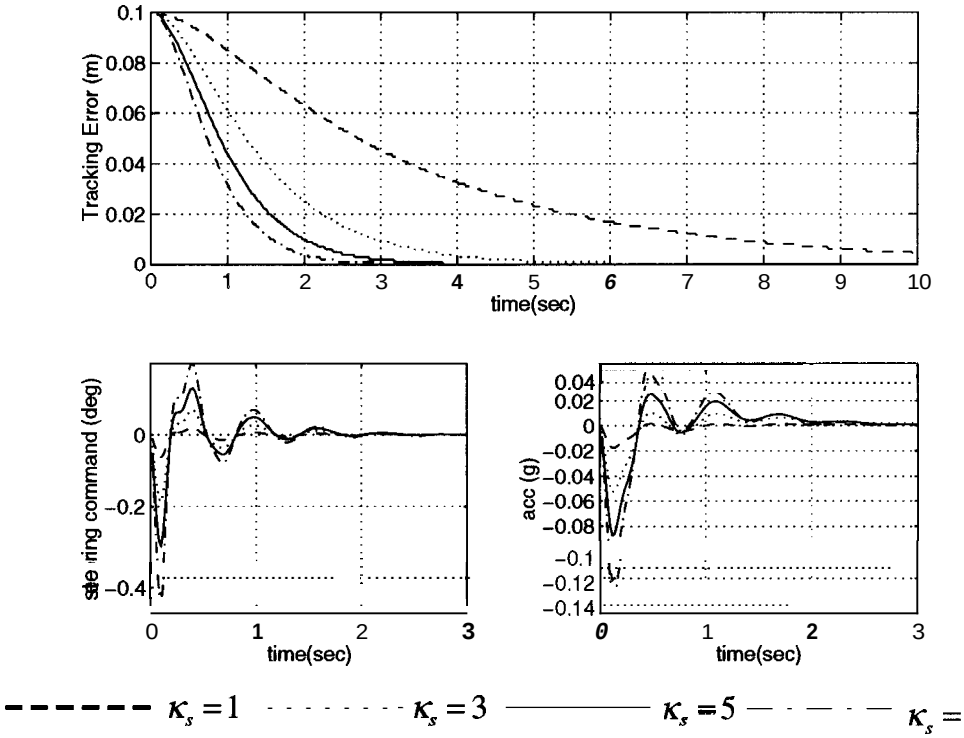

Figure 4.6: Convergence Test (Initial Tracking Error =0.1m)

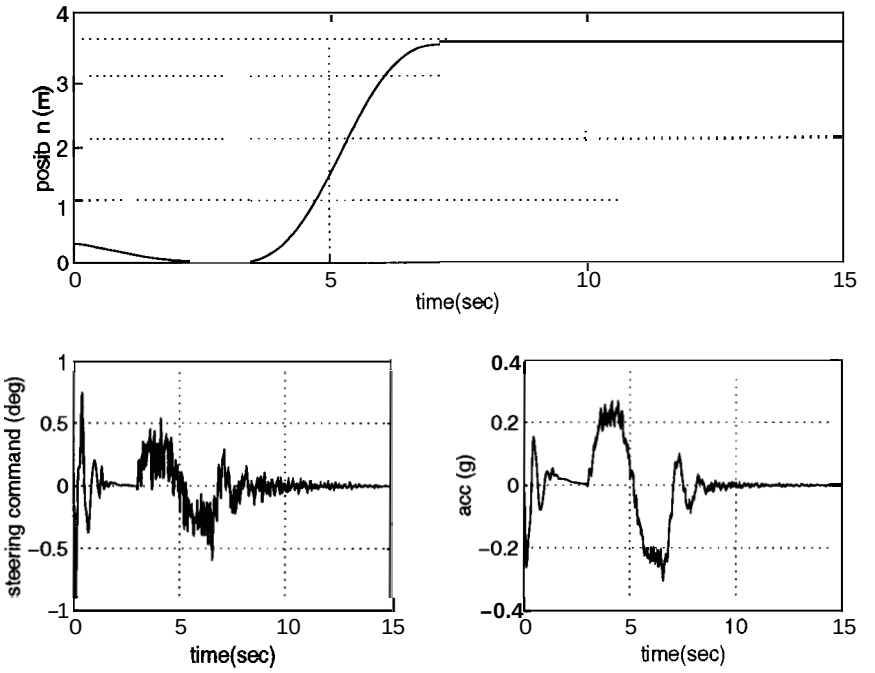

Figure 4.7: Multi-Maneuver Performance (Nominal Road Condition)

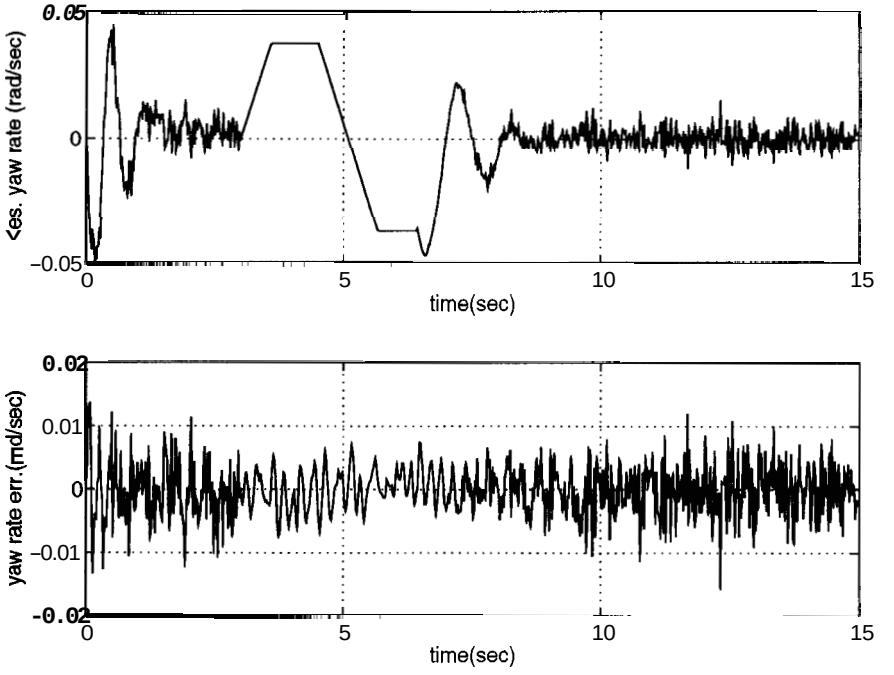

Figure 4.8: Yaw Rate Tracking Performance (Nominal Road Condition)

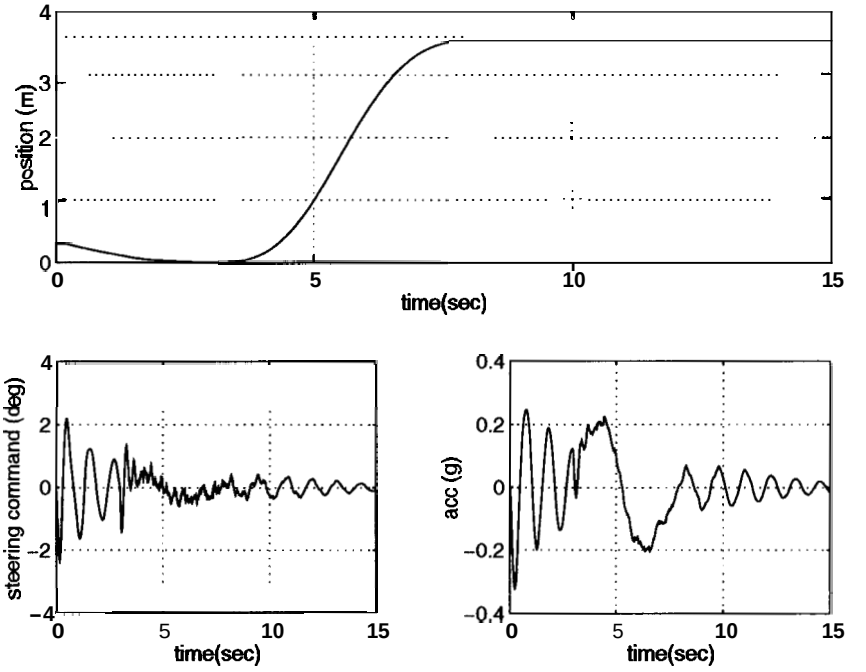

Figure 4.9: Multi-Maneuver Performance (Slippery Road with Wind)

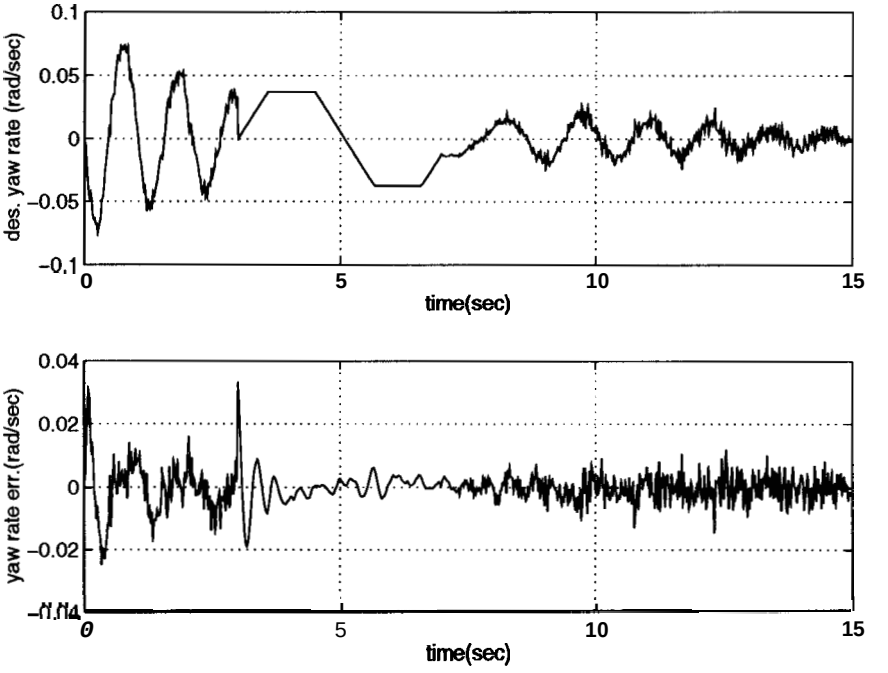

Figure 4.10: Yaw Rate Tracking Performance

(Slippery Road with Wind)

4.7 Summary

The unified lateral guidance algorithm has been introduced in this chapter. This algorithm consists of two parts: one is the desired yaw rate generator, and the other is the yaw rate tracking controller. The desired yaw rate tracking controller was obtained by Lyapunov design. The desired yaw rate for lane following maneuvers under **PATH** scenario and for lane change maneuvers were presented. **A** smooth transition between the lane change maneuvers and the lane following maneuvers was proposed. The stability of the overall system was proven. Simulations were conducted to validate the proposed algorithm. The simulations demonstrated the roboustness of the proposed scheme to the plant uncertainties such as road surface condition and wind disturbance.

Chapter 5

Conclusions and Future Research

5.1 Conclusions

This report has investigated the lateral guidance of a vehicle under PATH scenario: i.e., the road reference system composed of road-embedded magnets, on-board magnetometers and on-board inertia measurement sensors (a yaw rate sensor and an accelerometer).

The focus of the research was placed on the lane change maneuvers of the lateral guidance and two strategies for the lane change maneuvers were studied. In the first strategy, the lane change maneuvers were accomplished by constructing a tracking control system. The desired trajectory, called VDT, to be tracked by the control system was designed by including the ride comfort parameters (lateral acceleration limit and lateral jerk limit) explicitly. In Chapter 2, we have investigated the relations between the maneuver time and the ride comfort parameters, and provided a graphical way of designing the VDT. In Chapter **3,** we proposed a tracking controller to follow the VDT. **A** sliding mode controller was designed with respect to the frequency-weighted tracking error in order to enhance ride quality. Since the tracking controller designed in Chapter 3 was a state feedback controller, a state estimation was provided. This methodology was validated by the results of experiments with a prototype vehicle.

As the second strategy for the lane change maneuvers under the first scenario, the unified lateral guidance algorithm was proposed in Chapter 4. The unified lateral guidance algorithm consisted of the desired yaw rate generator and the yaw rate tracking controller. The desired yaw rate generator computed the desired yaw rate of a vehicle to achieve the desired maneuver, either lane change or lane following maneuver. We could achieve the desired maneuver by tracking the desired yaw rate through the action of the yaw rate tracking controller. Thus, the controller design can be designed separately, regardless of the maneuver. The desired yaw rates were obtained from the analysis of the kinematics of the desired maneuvers. The stability of the closed loop system was proven via the Lyapunov stability theory. The effectiveness of the algorithm was verified by the simulations.

5.2 Future Research

The following topics are recommended for future research:

- The results of the unified lateral guidance algorithm need to be verified experimentally. The experimental procedure should include the variations of operating conditions in longitudinal velocity and road surface.
- Yaw rate tracking controller: a robust controller, an adaptive controller, or other intelligent controller can be investigated to improve the performance.
- Combination of the magnet based road reference system and the vision system will provide reliable, accurate, and robust measurements of both the road and the vehicle over a wide range of operations including lane following and lane changing.

Bibliography

[1] Ackermann, J., Sienel, W., "Robust Control for Automatic Steering," *Proceedings of the American Control Conference,* San Diego, CA, pp. 795-800, 1990.

[2] Ackermann, J., Bartlett, A., Kaesbauer, D., Sienel, W., Steinhauser, R., Robust Control: Systems with Uncertain Physical Parameters, London, *Springer-Verlag,* 1993.

[3] Ackermann, J., Guldner, J., Sienel, W., Steinhauser, R., Utkin, V. I., "Linear and Nonlinear Controller Design for Robust Automatic Steering," *IEEE Trans. on Control System Technology,* Vol. 3, No. 1, pp.132-143, 1995.

[4] Caywood, W. C., Donnelly, H. L., Rubinstein, N., Guideline for Ride-Ouality Specifications Based on Transpo '72 test data; Johns Hopkins University Applied Physics Laboratory, technical report, UMTA-MD-06-0022-77-3, 1977.

[5] Chee, W., Tomizuka, M., "Vehicle Lane Change Maneuver in Automated Highway Systems," *Publication of PATH project,* ITS, UC Berkeley, UCB-ITS-PRR-94-22, 1994.

[6] Chee, W., Tomizuka, M., "Lane Change Maneuver of Automobiles for The Intelligent Vehicle and Highway System(IVHS)," *Proceedings of the American Control Conference,* Baltimore, MD, pp. 3586-3587, 1994.

r71 Chee, W., Tomizuka, M.., Patwardhan, S., Zhang, W., "Experimental Study of Lane Change Maneuver for AHS Applications," *Proceedings of the American Control Conference,* Seattle, WA, pp. 139-143, 1995.

[8] Conover, G. D., "The Eleven Commandments for IVHS," *Proceedings of Vehicle Navigation and Information Systems Conference,* pp. 503-506, 1994.

[9] Fenton, R. E., Melocik, G. C., Olsen, K. W., "On the Steering of Automated Vehicles: Theory and Experiment," *IEEE Trans. on Automatic Control,* Vol. 21, No. 3, pp. 306–315, 1976.

[10] Fenton, R. E., "IVHS/AHS: Driving into the future," *IEEE Control Systems Magazine,* Vol. 14, No. 6, pp. 13–20, 1994.

[11] Gardels, K., "Automatic Car Controls for Electronic Highway," GMR-276, *General Motors Corps.,* Warren, MI, 1960.

[12] Godthelp, J., van der Horst, A. R. A., Burrij S., van de Lagemaat, C., "Open and Closed Loop Steering in a Lane Change Maneuver," *Institute for Perception: National Defense Research Organization TNO group,* 1983.

[13] Hess, R.A.,. Modjtahedzadeh, A., "A Preview Control Model of Driver Steering Behavior," *Proceedings of IEEE International Conference on Systems, Man and Cybernetics,* Vol. 2, Cambridge MA, pp. 504–509, 1989.

[14] Hess, R.A.,. Modjtahedzadeh, A., "A Control Theoretic Model of Driver Steering Behavior," *IEEE Control System Magazine,* Vol. 10, No. 5, pp. 3–8, 1990.

[15] Hessburg, T., Lee, M.,. Takagi, H., Tomizuka, M., "Automatic Design of Fuzzy Systems using Genetic Algorithms and its Application to Lateral Vehicle Guidance," *Proceedings of Society of Photo-Optical Instrumentation Engineers (SPIE'93),* 1993.

[16] Hessburg, T., Peng, H., Zhang, W., Arai, A., Tomizuka, M., "Experimental Results of Fuzzy Logic Control for Lateral Vehicle Guidance," Publication of PATH project, ITS, UC Berkeley, UCB-ITS-PRR-94-03, 1993.

[17] Kailath, T., Linear Systems, Englewood Cliff, New Jersey, *Prentice-Hall,* 1980.

[18] Kalman, R. E., Bertram, J. E., "Control System Analysis and Design Via a the Second Method of Lyapunov. II Discrete-Time Systems," *Trans. of the ASME,* Vol. , pp. 394–400,1960.

[19] Krstic, M., Kanellakopoulos, I., Kokotovic, P., Nonlinear and Adaptive Control Design, New York, *John Wiley & Sons, Inc.,* 1995.

[20] Lugner, P., "Horizontal Motion of Automobiles - Theoretical and Practical Investigations," Dynamics of High-Speed Vehicles, New York, *Springer-Verlag,* 1982.

[21] Modjtahedzadeh, A., Hess, R. A., "A Model of Driver Steering Control Behavior for Use in Assessing Vehicle Handling Qualities," *ASME Journal of Dynamic Systems, Measurement, and Control,* Vol. 115, No. 3, pp. 456–464, 1993.

[22] Özgüner, Ü., Unyeliog'lu, **K.** A., Hatipog'lu, C., "An Analytical Study of Vehicle Steering Control," *Proceeding of the 4th IEEE Conference on Control Applications,* Albany, NY, pp.125–130, 1995.

[23] Pappas, ***G.*** J., Kyriakopoulos, K. J., "Dynamic Modeling and Tracking Control of Nonholonomic Wheeled Vehicles," *Proceedings of the IFAC,* Vol. 2, pp.241-244, 1993.

[24] Pacejka, H. B., Bakker, E., "The Magic Formula Tyre Model," *Proceedings of 1st International Colloquium on Tyre Models for Vehicle Dynamics Analysis,* Delft, Netherlands, pp. 1–18, 1991.

[25] Peng, H., Tomizuka, M., "Vehicle Lateral Control for Highway Automation," *Proceedings of the American Control Conference,* San Diego, **CA,** pp. 788–793, 1990.

[26] Peng, H., Tomizuka, M., "Lateral Control of Front-Wheel-Steering Rubber-Tire Vehicles, "Publication of PATH project, ITS, UC Berkeley, UCB-ITS-PRR-90-5, 1990.

[27] Peng, H., Tomizuka, M., "Preview Control for Vehicle Lateral Guidance in Highway Automation," *Proceedings of the American Control Conference,* Boston, MA, pp. 3090–3095,1991.

[28] Peng, H., Hessburg, T., Tomizuka, M., Zhang, M., Lin, Y., Devlin, P., Shladover, **S.** E., **Arai,** A., **"A** Theoretical and Experimental Study on Vehicle Lateral Control," *Proceedings of the American Control Conference,* Chicago, Illinois, pp. 1738–1742,1992.

[29] Pham, H. A., Hedrick, J. K., Tomizuka, M., "Combined Lateral and Longitudinal Control of Vehicles for Intelligent Highway Systems," *Proceedings of the American Control Conference,* Baltimore, MD, pp. 1205–1206, 1994.

[30] Praly, L., d'Andrea-Novel, **B.,** Coron, J. M., "Lyapunov Design of Stabilizing Controller for Cascaded Systems," *ZEEE Trans. on Automatic Control,* Vol. 36, No. 10, pp. 1177–1181, 1991.

[31] Segel, L., "Theoretical Prediction and Experimental Substantiation of the Response of the Automobile to Steering Control," *Automobile Division, The Institute of Mechanical Engineers,* pp. 26–46, 1956.

[32] Shladover, S. E., Wormley, D. N., Richardson, H. **H.,** Fish, **R.,** "Steering Controller Design for Automated Guideway Transit Vehicles," *ASME Journal of Dynamic System, Measurement and Control,* Vol. 100, No. 3, pp. 1–8, 1978.

[33] Shladover, S. E., "Research and Development Needs for Advanced Vehicle Control Systems," *IEEE MICRO,* Vol. 13, No. 1, pp. 11–19, February 1993.

[34] Slotine, J.E., Li, W., Applied Nonlinear Control, Englewood Cliff, New Jersey, *Prentice-Hall,* 1991.

[35] Utkin, V. **I.,** "Sliding Mode Control in Discrete-Time and Difference Systems," Variable Structure and Lyapunov Control (A. **S.** I. Zinober, ed.), London, U. **K.,** *Springer-Verlag,* pp. 83–103, 1993.

[36] Utkin, V. I., "Variable Structure Systems with Sliding Modes," *IEEE Trans. on Automatic Control,* Vol. 22, No. 2, **pp.** 212–222, 1977.

[37] Wong, J. Y., Theory of Ground Vehicles, *John Wiley & Sons Znc.,* 1993.

[38] Yonezawa, **K.,** "Reduced-Order Kalman Filtering with Incomplete Observability," *Journal of Guidance and Control,* Vol. 3, No. 3, pp. 280~282, 1980.

[39] Young, **K.** D., Özgüner, U., "Frequency Shaping Compensator Design for Sliding Mode," *International Journal of Control,* Vol. 57, No. 5, pp. 1005–1019, 1993.

[40] Zhang, W., R. Parsons, West, T., *"An* Intelligent Roadway Reference System for Vehicle Lateral Guidance/Control," *Proceedings of the American Control Conference,* San Diego, CA, pp. 281–286, 1990.

[41] "California PATH 1996 Annual Report," *California PATH,* Richmond CA, 1996.

Appendices

Review of Stability Theory

In the design of control system, we resort to Lyapunov theory for its stability proof. This section will summarize the Lyapunov stability theory and the related convergence theorems.

In the following formulations, $\mathbf{R}^n$ denotes an n-dimensional linear vector space over the reals with the norm $\|\cdot\|$. Let $\mathbf{R}_+ = [0,\infty)$.

Consider the nonautonomous system

$$\dot{x} = f(x,t) \tag{A.1}$$

where $f : \mathbf{R}^n \times \mathbf{R}_+ \to \mathbf{R}^n$ is locally Lipschitz in x and piecewise continuous in t.

Definition A.1 : (Equilibrium Point)

The origin $x = 0$ is the ***equilibrium*** point **for (A.1) if**

$$f(0,t) = 0, \quad \forall t \geq 0. \tag{A.2}$$

Definition A.2 : (Class K)

A continuous function $\gamma: [0,a) \to \mathbf{R}_+$ is said to belong to ***class*** $\mathcal{K}$ if it is strictly increasing and $\gamma(0) = 0$. It is said to belong to ***class*** $\mathcal{K}_\infty$ if $a = \infty$ and $\gamma(r) \to \infty$ as $r \to \infty$.

Definition A.3 : (Class KL)

A continuous function $\beta : [0,a) \times \mathbf{R}_+ \to \mathbf{R}_+$ is said to belong to ***class*** KL if for each fixed s the mapping $\beta(r,s)$ belongs to ***class*** K with respect to r, and for each fured s the mapping $\beta(r,s)$ is decreasing with respect to s and $\beta(r,s) \to 0$ as $s \to \infty$. It is said to belong to ***class*** KL_∞ if, in addition, for each fured s the mapping $\beta(r,s)$ belongs to ***class*** K_∞ with respect to r.

A.1 Lyapunov Stability Theory

In the Lyapunov stability theory, the following definition of the stability of the equilibrium point is considered.

Definition A.4 : (Stability)

The equilibrium point $x = 0$ of **(A.1)** is

- ***uniformly stable,*** if there exists a ***class*** K function $\gamma(\cdot)$ and a positive constant c, independent of t_0, such that

$$\|x(t)\| \le \gamma(\|x(t_0)\|), \quad \forall t \ge t_0 \ge 0, \quad \forall x(t_0): \|x(t_0)\| < c; \tag{A.3}$$

- ***uniformly asymptotically stable,*** if there exists a ***class*** KL function $\beta(\cdot,\cdot)$ and a positive constant ***c,*** independent of t_0, such that

$$\|x(t)\| \le \beta(\|x(t_0)\|, t - t_0), \quad \forall t \ge t_0 \ge 0, \quad \forall x(t_0): \|x(t_0)\| < c; \tag{A.4}$$

- ***exponentially stable,*** if **(A.4)** is satisfied with $\beta(r,s) = kre^{-\alpha s}$, $k > 0$, $\alpha > 0$;
- ***globally uniformly stable,*** if **(A.3)** is satisfied with $\gamma \in K_\infty$ for any initial state $x(t_0)$;
- ***globally uniformly asymptotically stable,*** if **(A.4)** is satisfied with $\beta \in KL_\infty$ for any initial state $x(t_0)$; and
- ***globally exponentially stable,*** if **(A.4)** is satisfied with for any initial state $x(t_0)$ with $\beta(r,s) = kre^{-\alpha s}$, $k > 0$, $\alpha > 0$.

Then, the main Lyapunov stability theorem is formulated as follows.

Theorem A.5 : (Uniform Stability)

Let $x = 0$ be an equilibrium point of (A.l) and $\mathbf{D} = \{x \in \mathbf{R}^n : \|x\| < r\}$. Let $V : D \times \mathbf{R}_+ \to \mathbf{R}_+$ be a continuously differentiable function such that, $\forall t \geq 0$, $\forall x \in \mathbf{D}$,

$$\gamma_1(\|x\|) \leq V(x,t) \leq \gamma_2(\|x\|) \tag{A.5}$$

$$\frac{\partial V}{\partial t} + \frac{\partial V}{\partial x} f(x,t) \leq -\gamma_3(\|x\|), \tag{A.6}$$

Then, the equilibrium is

- *uniformly stable,* if γ_1 and γ_2 are *class* K functions on $[0,r)$ and $\gamma_3(\cdot) \geq 0$ on $[0,r)$;
- *uniformly asymptotically stable,* if γ_1, γ_2 and γ_3 are *class* K functions on $[0,r)$;
- *exponentially stable,* if $\gamma_i(\rho) = k_i \rho^{\alpha}$, $k_i > 0$, $a > 0$, $i = 1, 2, 3$ on $[0,r)$;
- *globally uniformly stable,* if $\mathbf{D} = \mathbf{R}^n$, γ_1 and γ_2 are *class* K_{∞} functions, and $\gamma_3(\cdot) \geq 0$ on $\mathbf{R}_+$;
- *globally uniformly asymptotically stable,* if $D = \mathbf{R}^n$, γ_1 and γ_2 are *class* K_{∞} functions, and γ_3 is a *class* K function on $\mathbf{R}_+$; and
- *globally exponentially stable,* if $D = \mathbf{R}^n$ and $\gamma_i(\rho) = k_i \rho^{\alpha}$, $k_i > 0$, $a > 0$, $i = 1, 2, 3$ on $\mathbf{R}_+$.

A.2 Convergence Theorems

Lemma A.6: (Barbalat)

Consider the function $\phi : \mathbf{R}_+ \to \mathbf{R}$. If ϕ is uniformly continuous and $\lim_{t \to \infty} \int_0^t \phi(\tau) d\tau$ exists and is finite, then

$$\lim_{t\to\infty}\phi(t)=0. \tag{A.7}$$

Theorem A.7: (La Salle-Yoshizawa)

Let $\mathbf{x}=0$ be an equilibrium point of **(A.l)** and suppose f is locally Lipschitz in $\mathbf{x}$ uniformly in t. Let V: $\mathbf{R}^n \times \mathbf{R}, \to \mathbf{R},$ be a continuously differentiable function such that

$$\gamma_1(\|x\|)\le V(x,t)\le \gamma_2(\|x\|) \tag{A.8}$$

$$\frac{\partial V}{\partial t}+\frac{\partial V}{\partial x}f(x,t)\le -W(\|x\|)\le 0 \tag{A.9}$$

$\forall t\ge 0,\ \forall x \in \mathbf{R}^n$, where γ_1 and γ_2 are class K_∞ functions and W is a continuous function. Then, all solutions of **(A.l)** are globally uniformly bounded and satisfy

$$\lim_{t\to\infty}W(x(t))=0. \tag{A.lO}$$

In addition, if $W(x)$ is positive definite, then the equilibrium $\mathbf{x}=0$ is globally uniformly asymptotically stable.

A.3 Lyapunov-Based Control

One objective of control design is *to* create closed-loop systems with desirable stability properties. Thus, it is desired to extend the Lyapunov function concept to the control Lyapunov function([19][30]).

Suppose that our problem for the time-invariant system

$$\dot{x}=f(x,u),\ x\in\mathbf{R}^n,\ u\in\mathbf{R}, f(0,0)=0, \tag{A.11}$$

is to design a feedback control law $\alpha(x)$ for the control variable u such that the equilibrium point $\mathbf{x}=0$ of the closed-loop system

$$\dot{x}=f(x,\alpha(x)) \tag{A.12}$$

is globally asymptotically stable. We can choose a function $V(x)$ as a Lyapunov candidate, and require that its derivative along the solutions of (A.12) satisfy

$\dot{V}(x) \le -W(x)$, where $W(x)$ is a positive definite function. Thus, it is needed to find $\alpha(x)$ to guarantee that

$$\frac{\partial V}{\partial x} f(x, \alpha(x)) \le -W(x). \tag{A.13}$$

Definition A.8: (Control Lyapunov Function)

A smooth positive definite and radially unbounded function $V: \mathbf{R}^n \to \mathbf{R}_+$ is called a ***control Lyapunov function*** for **(A.11)** if

$$\inf_{u \in \mathbf{R}} \left\{ \frac{\partial V}{\partial x} f(x, u) \right\} < 0, \quad \forall x \neq 0 \tag{A.14}$$